

# University of Alberta

Microstructural Characterization of Asphaltenes on Surfaces

by

Mahsa Mehranfar

A thesis submitted to the Faculty of Graduate Studies and Research  
in partial fulfillment of the requirements for the degree of

Master of Science

in

Chemical Engineering

Department of Chemical and Materials Engineering

©Mahsa Mehranfar  
Spring 2014  
Edmonton, Alberta

Permission is hereby granted to the University of Alberta Libraries to reproduce single copies of this thesis and to lend or sell such copies for private, scholarly or scientific research purposes only. Where the thesis is converted to, or otherwise made available in digital form, the University of Alberta will advise potential users of the thesis of these terms.

The author reserves all other publication and other rights in association with the copyright in the thesis and, except as herein before provided, neither the thesis nor any substantial portion thereof may be printed or otherwise reproduced in any material form whatsoever without the author's prior written permission.

## **Dedication**

This thesis is dedicated to my parents  
For their love, endless support and encouragement

## **Abstract**

Crude oils contain a distribution of molecules with diverse chemical structures and molecular weights. Asphaltenes are considered the most problematic of these structures. We have investigated the adsorption and aggregation of asphaltenes on surfaces using scanning probe microscopy. Modifying the chemical properties of surfaces using self-assembled monolayers (SAM) can change the wettability and adsorption characteristics of molecules. We have investigated adsorption of asphaltenes on gold substrates modified using dodecanethiol SAM. The molecular characteristics and thickness of the monolayers were determined using Fourier Transform infrared (FT-IR) spectroscopy and ellipsometry, respectively. The results showed that SAM inhibits the adsorption of asphaltenes on surface. To investigate the morphology of asphaltene aggregates, we used atomic force microscopy (AFM). In addition to qualitative observations of structural changes, quantitative changes in adhesion and contact potential differences ( $V_{CPD}$ ) of asphaltene aggregates as a function of temperature were also carried out.

## **Acknowledgement**

During my studies as a Masters student, many individuals have helped me and I take this opportunity to briefly express my gratitude to all for everything they have done. Without them the fulfillment of this project would not have been possible.

My deepest and sincere gratitude to my supervisor, Prof. Thomas Thundat, for believing in me and giving me the opportunity to work in his group and laboratory as well as encouraging and guiding me with his vast knowledge and great enthusiasm for science and research. This thesis, in its current form, would not have been possible without his leadership, persistence and encouragement. It was his guidance that enabled me to overcome the challenges of my research. He also showed honest interest inquiring about how I was doing in my personal life and advised me accordingly. I knew that I could always count on him.

I would like to express my gratitude to Dr. Ravi Gaikwad for training me and helping me to run AFM experiments and also for providing me valuable advice and guidance throughout this research.

I am especially grateful to Prof. Sushanta Mitra and Dr. Siddhartha Das of Mechanical Engineering for their great comments, ideas and suggestions during my project. They deserve my sincere gratitude. I would also like to thank Prof. Murray Gray for providing me with ‘Asphaltene’ samples for my research.

I would also like to thank my best friend, Amin Pourmohammadbagher, who took his time out to painstakingly proofread my thesis. My sincere gratitude goes to him for being with me through all the sad and happy moments. I wish to thank all the group members of “Nano Interfaces & Molecular Engineering” (NIME) with whom I worked for two years and I wish them all the success and happiness in the world. I really appreciate the assistance and support from Ms. Elizabeth Adolf and

Ms. Lily Laser during my Masters tenure here. I want to acknowledge the Canada Excellence Research Chair (CERC) program for the financial support during my Master's program.

Last, but not the least, I would like to thank my family members for their unconditional love and support. Their constant encouragement instilled in me the confidence required to successfully complete this work. Finally, I am thankful to my brother, Mahyar, for encouraging me to pursue my Masters in the first place and also for all the support he has given me. No words can express my love for him.

Thank you all!

# Table of Contents

## CHAPTER 1

<b>INTRODUCTION .....</b>	<b>1</b>
1.1. Oil Sands .....	1
1.2. An Overview on Asphaltenes .....	3
1.2.1. Definition .....	3
1.2.2. Self-Association Behaviour .....	3
1.2.3 Chemical Composition.....	4
1.2.4. Structure .....	5
1.2.5. Molecular Weight .....	7
1.2.6. Models.....	8
1.2.7. Electrical Charge of Asphaltenes .....	12
1.2.8. Summary .....	13
1.2.9. Thesis Outline .....	14

## CHAPTER 2

<b>ADSORPTION OF ASPHALTENES ON SELF-ASSEMBLED MONOLAYERS OF DODECANETHIOL ACCESSED BY FT-IR AND ELLIPSOMETRY.....</b>	<b>16</b>
2.1. Self-Assembly Monolayer (SAM).....	19
2.2. Experimental Methods .....	21
2.2.1. Materials and Chemicals .....	21
2.2.2. Asphaltenes Preparation.....	21
2.2.3. Solution preparation.....	22
2.2.4. Sample preparation .....	23
2.2.5. FT-IR Measurements .....	26
2.2.5.1. Dodecanethiol on Gold Substrate .....	26
2.2.5.2. Asphaltenes on Gold Substrate .....	28
2.2.5.3. Asphaltenes on SAM-Coated Gold Substrate .....	29
2.2.6. Ellipsometry Measurements.....	30

**CHAPTER 3**

**AFM MEASUREMENTS ..... 34**

- 3.1. An Overview on Atomic Force Microscopy (AFM) ..... 34
- 3.2. An Overview on Kelvin Probe Force Microscopy (KPFM) ..... 39
- 3.3. Materials and Methods ..... 41
  - 3.3.1. Asphaltenes Preparation..... 42
  - 3.3.2. Solution Preparation..... 42
  - 3.3.3. Depositing of Asphaltenes on SiO<sub>2</sub> Wafer Surface ..... 42
- 3.4. Results and Discussion..... 43

**CHAPTER 4**

**CONCLUSION AND FUTURE WORK ..... 58**

**Literature Cited ..... 60**

## List of Tables

Table 1. Elemental composition of bitumen and asphaltene precipitated from n-heptanes (Taken from reference 27). .....	5
Table 2. Composition of the asphaltene sample (Taken from reference 73). .....	21
Table 3. Peak position for $\text{CH}_3(\text{CH}_2)_{11}\text{SH}$ .....	28
Table 4. Film thickness (in Å) on gold-coated substrate as determined by ellipsometry.....	32

## List of Figures

Figure 1. SARA fractionation. ....	1
Figure 2. Two possible models for the asphaltenes structure: a) Island model, composed of one fused aromatic core surrounded by aliphatic chains (left), b) archipelago model, multiple aromatic cores interconnected by aliphatic chains. (right) (Taken from reference <sup>33</sup> ). ....	6
Figure 3. Several molecular structures that have been recommended for asphaltenes and resins based on island and archipelago models (Taken from reference <sup>34</sup> ). ....	7
Figure 4. 125 common core structures in petroleum fractions boiling up through five condensed aromatic ring structures (Taken from reference 40). ....	9
Figure 5. ○ resin molecules, ● aromatic molecules, — oil molecules,  asphaltene particles. Resins are adsorbed on the asphaltene surface and cause the asphaltenes to be stabilized due to the repulsion between resins that adsorbed on asphaltene surface and resins in the solution (Taken from reference <sup>41</sup> ). ....	10
Figure 6. Polymer-like aggregates of asphaltenes. In this model, asphaltenes have single or multiple active sites and act as propagators and resins have single active sites and act as terminators (Taken from reference 42). ....	11
Figure 7. Schematic representation of a supramoleculal assembly. Molecular interactions are: acid-base interactions and hydrogen bonding (blue), metal coordination complexes (red), hydrophobic pockets (orange) and aromatic pi-pi stacking (green) (Taken from reference 43). ....	12
Figure 8. Summarized asphaltenes' properties. ....	14
Figure 9. Asphaltene deposition in a pipeline. ....	18
Figure 10. Chemical structure of dodecanethiol. ....	19

Figure 11. Schematic of two structural models of self-assembly: a) closed-packed arrangement of alkyl chain and sulfur head groups oriented normal to the solid surface, b) closed-packed arrangement of alkyl chain and sulfur head groups oriented at an angle $\phi$ from the surface. The yellow substrate, red circles and blue bars correspond to gold, sulfur head groups and alkane chains, respectively. ....	20
Figure 12. Asphaltenes sample. ....	22
Figure 13. Asphaltene/toluene solution. ....	22
Figure 14. Schematic of SAM preparation. The yellow substrate, red circles and blue bars correspond to gold, sulfur head groups and alkane chains, respectively. In the first stage (a), a low density “striped” phase is formed. This is followed by an “intermediate” stage (b) and finally, in the “standing up” phase (c), a closed-pack oriented monolayer is formed on the surface. ....	24
Figure 15. Different types of surface defects. The yellow substrate, red circles and blue bars correspond to gold, sulfur head groups and alkane chains, respectively. ....	25
Figure 16. FTIR absorption spectrum peaks of dodecanethiol on gold substrate. Peaks between $2800\text{ cm}^{-1}$ and $3000\text{ cm}^{-1}$ correspond to absorption by $\text{CH}_3$ and $\text{CH}_2$ bonds of alkane chain. ....	27
Figure 17. FTIR spectra of the asphaltenes on gold substrate. ....	28
Figure 18. FT-IR absorption spectrum peaks of asphaltene on SAM-coated substrate. Peaks between $2800\text{ cm}^{-1}$ and $3000\text{ cm}^{-1}$ correspond to absorption by $\text{CH}_3$ and $\text{CH}_2$ bonds of alkane chain. ....	30
Figure 19. Schematic of ellipsometry experiment. ....	31
Figure 20. Schematic of asphaltene adsorbed on a) dodecanethiol modified and b) gold coated substrate. The yellow substrate, red circles and blue bars correspond	

to gold, sulfur head groups and alkane chains, respectively. Asphaltene aggregates are shown in black.....	32
Figure 21. Schematics of an atomic force microscopy. It consists of a sharp tip mounted at the end of a flexible cantilever, a piezoelectric element, laser diode, and photodetector.....	35
Figure 22. Topography images of sample 1, a) 5% (top), b) 50% (bottom). Thin films were heated up to 60 °C in stage I and to 120 °C in stage II, and after each stage, the samples were cooled down to 25 °C (Taken from reference <sup>85</sup> ). .....	37
Figure 23. Topography images of sample 2, a) 5% (top), b) 50% (bottom) (Taken from reference 85).....	38
Figure 24. Schematic depiction of KPFM .....	40
Figure 25. Control bare SiO <sub>2</sub> .....	43
Figure 26. The optical image of asphaltene aggregates in a peculiar pattern. The sample was heated in vacuum oven in 150 °C for about 2 hours.....	44
Figure 27. Topography of asphaltene on different locations of silicon wafer substrate, heated up to 150 °C for 2 hours. ....	45
Figure 28. (a) Silicon wafers were rinsed with ethanol and dried with N <sub>2</sub> gas, (b) A drop of asphaltenes/toluene solution was cast deposited on the silicon wafers, (c) Toluene was allowed to evaporate at ambient temperature for 30 minutes, (d) The samples were mounted on the heating element installed below the AFM tip. ....	47
Figure 29. Topographic AFM images at different temperatures (A) 25 <sup>0</sup> C, (B) 55 <sup>0</sup> C, (C) 65 <sup>0</sup> C and (D) 80 <sup>0</sup> C. A drop of asphaltene solution was cast deposited on the silicon wafer substrate and allowed to evaporate at room temperature. ....	48

Figure 30. Height distribution of asphaltenes aggregates at various temperatures. .....	50
Figure 31. The adhesion at temperatures (I) 25 <sup>0</sup> C, (J) 55 <sup>0</sup> C, (K) 65 <sup>0</sup> C and (L) 80 <sup>0</sup> C.....	51
Figure 32. The contact potential differences at temperatures (A) 25 <sup>0</sup> C, (B) 55 <sup>0</sup> C, (C) 65 <sup>0</sup> C and (D) 80 <sup>0</sup> C.....	52
Figure 33. Asphaltenes adhesion as a function of temperature.....	53
Figure 34. Contact potential difference ( $V_{CPD}$ ) between the AFM probe and asphaltene aggregates as a function of temperature (A), $V_{CPD}$ image of asphaltene aggregates (B) and cross section of image shown in B to identify dual distribution of $V_{CPD}$ for hair like and broader structures. The red and black arrows indicate lower and higher $V_{CPD}$ distribution respectively. ....	54
Figure 35. The specific heat capacities of asphaltenes for the first initial heating cycle 1 (red) and heating of the same sample after cooling it down back to room temperature cycle 2 (blue). Two glass transition temperatures were identified for the first heating cycle ( $T_{G1}=41^0C$ and $T_{G2}=60^0C$ ) and there is endothermic to exothermic phase transition at $T=75^0C$ . For the second heating cycle there may be several glass transition temperatures, but no endothermic to exothermic phase transition temperature. ....	56

## List of Abbreviations

SARA	Saturates-Aromatics-Resins-Asphaltenes
nC <sub>7</sub>	n-heptane
nC <sub>5</sub>	n-pentane
VPO	Vapor Pressure Osmometry
SAXS	Small-Angle X-ray Scattering
SANS	Small-Angle Neutron Scattering
ppm	Parts Per Million
CMC	Critical Micelle Concentration
g	Gram
l	Litre
AFM	Atomic Force Microscopy
UV-Vis	Ultraviolet-Visible
MW	Molecular Weight
FIMS	Field Ionization Mass Spectroscopy
SEC	Size Exclusion Chromatography
wt%	Weight %
PSD	Position Sensitive Photodiode Detector
SEM	Scanning Electron Microscopy
TEM	Transmission Electron Microscopy
rpm	Revolutions Per Minute
S	Second
°C	Degree Celsius
DLA	Diffusion Limited Aggregation
KPFM	Kelvin Probe Force Microscopy
NC	Non-Contact
CPD	Contact Potential Difference
$\Phi_{\text{sample}}$	Work function of sample
$\Phi_{\text{tip}}$	Work function of tip
e	Electronic charge
V <sub>AC</sub>	Alternating voltage

$V_{DC}$	Direct voltage
$F_{es}$	Electrostatic force
$z$	Direction normal to the sample surface
$\omega$	Frequency
$\frac{\partial C(z)}{\partial z}$	Capacitance gradient between tip and sample surface
$V$	Voltage
$t$	Time
PF-KPFM	Peak Force-Kelvin Probe Force Microscopy
Ni	Nickel
V	Vanadium
SAM	Self-Assembled Monolayer
CPD	Contact Potential Difference
DSC	Differential Scanning Calorimetry

# Chapter 1

## Introduction

### 1.1. Oil Sands

Oil sands, or bituminous sands, are the unconsolidated sand deposits found in large amounts in many countries throughout the world. Huge deposits exist in Venezuela and Canada (northern Alberta such as Athabasca, Cold Lake and Peace River). The oil sands consist of a 6-14 wt% viscous oil known as bitumen, 80-85 wt% mineral solids and the remaining few percent is water.

Bitumen is a complex mixture of many different chemicals. It contains hydrocarbons, solid particles and water. The hydrocarbons existing in bitumen, known as SARA (Figure 1), are characterized as saturates, aromatics, resins and asphaltenes. The remaining portion of bitumen is called maltene<sup>1</sup>. Overall 1.7 trillion barrels of bitumen has been discovered northern Alberta with 173 billion barrels of recoverable oil from oil sands.

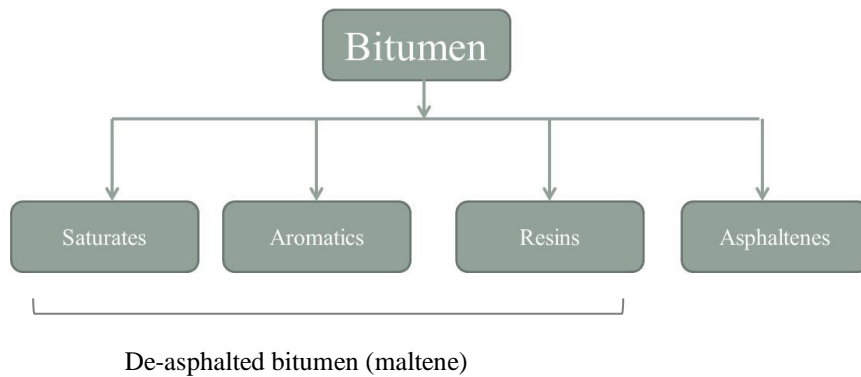


**Figure 1. SARA fractionation.**

In order to recover bitumen from the oil sands, a water-based extraction process is used. Oil sands are mixed with hot water and agitated with air to separate the bitumen. Bitumen recovered as froth from oil sands contains roughly 60 wt% bitumen, 30 wt% water and 10 wt% fine solids. In order to produce bitumen containing minimum water and fine solids, further treatment of froth is required. The bitumen density is decreased when they attach to air bubbles, therefore allowing them to be separated from water. After de-aeration, the froth is diluted by adding a solvent (e.g., paraffinic or naphthenic solvents) in order to reduce viscosity and increase the density difference between bitumen and water.

Paraffinic and naphtha diluents behave differently. In dilution of the bitumen with paraffinic diluents (i.e. hexane) due to low solubility of asphaltenes in alkane solvents, the solid particles and water droplets separate along with precipitated asphaltenes which enhances bitumen purity. Despite the high quality of bitumen produced by paraffinic solvent treatment, the attained bitumen yield is lower compared to that of a naphtha-based froth treatment since about 7% of the bitumen (i.e. asphaltenes) is precipitated. However, in naphtha-based froth treatment asphaltenes do not precipitate and, therefore, require the use of enhanced gravity separation method. When using naphtha as a diluent, the final product does not have the high quality<sup>2</sup>.

Asphaltenes precipitate upon addition of paraffinic solvents. They are also flocculated, which is the first step of precipitation, by pressure drop on certain live crude oils<sup>3</sup>. Precipitation of asphaltenes can result in equipment fouling, pipeline plugging, catalyst deactivation, etc. Therefore, asphaltenes are often considered as the most problematic portion of crude oil and oil sands. In the recent years, much research has been carried out in investigating asphaltenes in order to obtain a better understanding of their complex nature.

## 1.2. An Overview on Asphaltenes

### 1.2.1. Definition

Crude oils contain a distribution of molecules with diverse chemical structures and molecular weights<sup>4</sup>, of which asphaltenes are considered as the heaviest, most viscous and polar component. Asphaltenes do not have a precise chemical definition and are defined by their solubility characteristics. They are soluble in aromatic hydrocarbons such as toluene or benzene, but insoluble in saturated hydrocarbons such as pentane, hexane or heptane<sup>5-8</sup>. N-heptane (nC<sub>7</sub>) is the most widely used solvent for asphaltenes precipitation, but n-pentane (nC<sub>5</sub>) is also used for industrial scale applications.

### 1.2.2. Self-Association Behaviour

A major property of asphaltenes is their self-association in order to form aggregates. Asphaltenes have a tendency to form aggregates in crude oil and in solvents such as toluene since they contain a number of functional groups, forming macromolecules and precipitate<sup>9,10</sup>. This tendency has been attributed to the presence of acid-base interactions, hydrogen bonding, pi-pi stacking, steric repulsions from alkyl chains and electrostatic forces<sup>9,11</sup>. Self-association of asphaltenes can be evaluated using different experimental techniques such as molar mass measurements<sup>12</sup>, vapor pressure osmometry (VPO)<sup>13</sup>, fluorescence<sup>14</sup>, etc. However, as a result of the complex mixture of asphaltene, the size and structure of asphaltene monomers and aggregates and the mechanism of self-association are debatable.

Nano-aggregation is defined as aggregates of asphaltene with the sizes in the range of nanometer. The size of asphaltene aggregation was measured using

small-angle X-ray scattering (SAXS) and small-angle neutron scattering (SANS) in the range of 4-10 nm in a medium concentration of organic diluents<sup>15,16</sup>. Mullins and his co-workers also showed that aggregation size of asphaltene molecules at low concentration is in the range of 2-3 nm and they contain approximately 5 asphaltene molecules<sup>17</sup>. Membrane diffusion results by Dechaine and Gray also support these values<sup>18</sup>. Recent studies show that the aggregation of asphaltene molecules in toluene is initiated at concentration as low as 50-100 ppm<sup>17,19,20</sup>.

The temperature and concentration of asphaltene affects the size of self-association in different solvents. Increasing the temperature and decreasing the concentration of asphaltene result in smaller aggregates<sup>21</sup>. Pressure also affects the aggregation size of asphaltene, however, it is less significant than temperature on asphaltene aggregates<sup>22</sup>.

### **1.2.3 Chemical Composition**

Elemental composition is the most basic attribute of any chemical compound. Compared to other petroleum fractions, aromaticity, carbon to hydrogen ratio, oxygen, nitrogen, sulfur and metals content are higher in the asphaltene fraction. Asphaltenes elemental composition is well-defined and there is no controversy surrounding it. For asphaltene fractions separated from different sources, the heteroatom contents are different because of the localized variations in the plant and mineralogical composition of the geological formations<sup>2</sup>. However, ultimate compositions are remarkably constant.

For many crude oil samples, elemental analysis of the asphaltene shows that they are composed of carbon and hydrogen in an approximate 1 to 1.2 ratio, as well as a small percent of heteroatoms such as sulfur (2-6%), nitrogen (1-1.2 %), oxygen (0.8-2 %), vanadium (100-300 ppm) and nickel<sup>23,24</sup>. It has been revealed that the

main oxygen-containing groups of asphaltene are the hydroxylic, carboxylic and carbonyl groups<sup>25</sup>. The condensed aromatic sheets are connected by ether, sulfide, aliphatic chains, naphthenic ring linkages and heterocyclic atoms. Also, vanadium and nickel exist in the form of porphyrin by chelate or coordinate bonds<sup>23,26</sup>. Table 1 lists the elemental composition of Athabasca bitumen and the corresponding asphaltene precipitated from n-heptane<sup>27</sup>.

**Table 1. Elemental composition of bitumen and asphaltene precipitated from n-heptanes (Taken from reference 27).**

Element	Carbon	Hydrogen	Nitrogen	Sulfur	Oxygen	H/C
Asphaltenes, wt%	80.8	7.8	1.2	8.8	1.4	1.15
Bitumen, wt%	83.1	10.6	0.4	4.8	1.1	1.53

#### 1.2.4. Structure

Many studies have been conducted in order to determine the chemical structure of asphaltene and the mechanism that causes asphaltene to aggregate and precipitate out of crude oil. There is a large and ongoing debate on the structure of asphaltene, however two main molecular structures have been suggested for asphaltene in the literature:

- 1) The island model (continental model): Figure 2a shows three of the many possible asphaltene island structures. This model is composed of one fused aromatic core surrounded by aliphatic chains like fingers around the palm.
- 2) The archipelago model: this model is illustrated in Figure 2b, there are multiple aromatic cores are interconnected by aliphatic chains.

In order to discover the best structure for asphaltene molecules, researchers are still studying these two suggested molecular model compounds. These two

asphaltene molecule structures lead to different points of view of the self-association mechanism. Values reported in the literature<sup>28-31</sup> measure the critical micelle concentrations (CMC) for asphaltenes in different organic solvents and most values are in the range of 0.1-10 g/L. However, Rogel et al.<sup>28</sup> measured CMC values up to asphaltenes concentrations of 30 g/L. For some time, it was believed that the aggregation of asphaltene molecules is initiated above CMC. In fact, over the years considering CMC characteristics for asphaltene molecules, Merino-Garcia and Anderson<sup>32</sup> showed that asphaltenes undergo a stepwise aggregation/association as their concentration is increased in organic solvents. They also showed that the concept of critical micelle concentration was inferred from misinterpretation of the surface tension and does not fit the behavior of a micelle-like system.

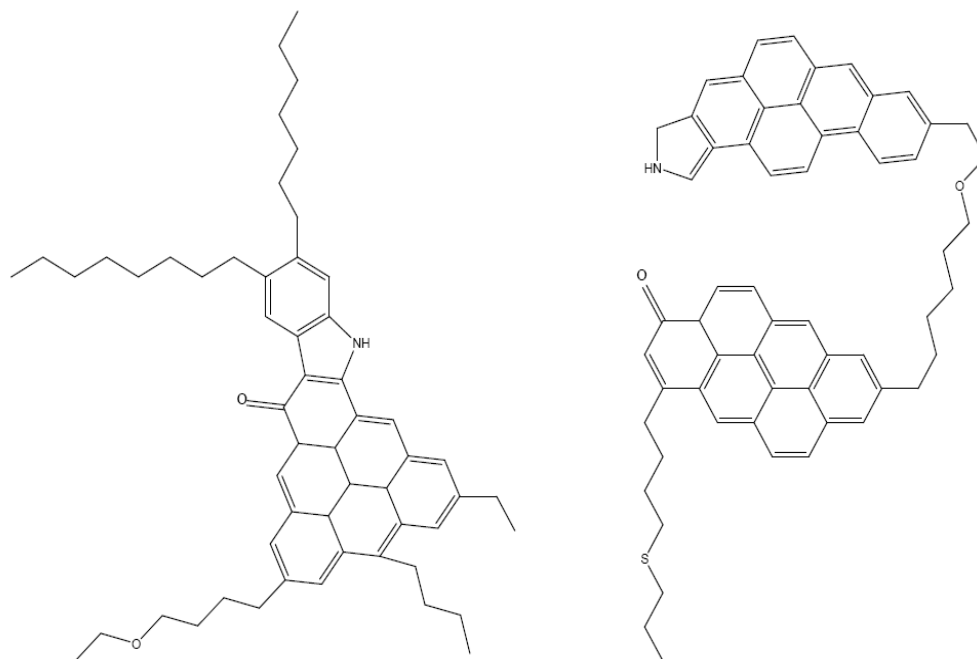


**Figure 2.** Two possible models for the asphaltenes structure: a) Island model, composed of one fused aromatic core surrounded by aliphatic chains (left), b) archipelago model, multiple aromatic cores interconnected by aliphatic chains. (right) (Taken from reference<sup>33</sup>).

Some of the molecular structures recommended for asphaltenes and resins based on these two models are shown in Figure 3<sup>34</sup>.

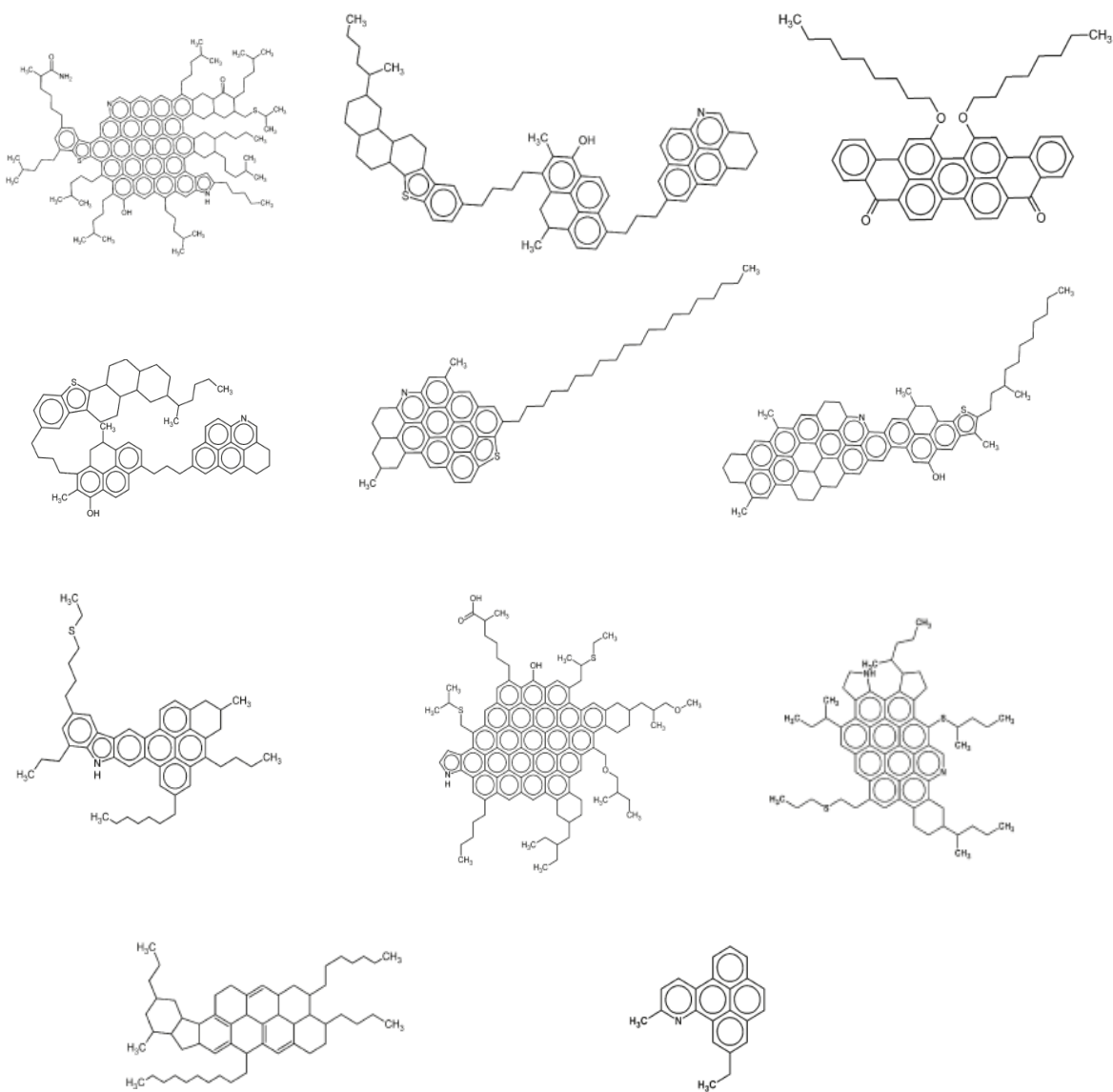


**Figure 3. Several molecular structures that have been recommended for asphaltenes and resins based on island and archipelago models (Taken from reference <sup>34</sup>).**

### 1.2.5. Molecular Weight

The molecular weight (MW) of asphaltene, which provides significant information about its characteristics, was controversial for many years since it yielded different values depending on the technique used. Asphaltene molecules

often have a tendency to aggregate, making MW difficult to determine. Several methods have been used, in order to determine the molecular mass of asphaltene. For example, the molecular weight of asphaltene obtained using the vapor pressure osmometry (VPO) technique is a reported 4000 daltons, however, field ionization mass spectroscopy (FIMS) has indicated a lower molecular weight in the range of 800 daltons<sup>35</sup>. Size exclusion chromatography (SEC) results have given a molecular weight as high as 10000 daltons<sup>36</sup>. Now, seems to be established that average molecular weight of about 750 daltons, with a full width at half maximum of 500-1000 daltons<sup>20,37</sup>.

### **1.2.6. Models**

Since the knowledge of asphaltenes' chemical and physical characteristics are limited as a result of their unknown molecular structure, various studies have been done to model asphaltenes using compounds having similar physicochemical properties. Since the model compounds have well defined structures with known properties, working with them is much easier than working with asphaltenes. For instance Schneider et al.<sup>38</sup> used perylene and porphyrine as asphaltene model compounds for studying the molecular weight of asphaltenes by fluorescence technique. Nordgard and his coworkers<sup>39</sup> used polyaromatic compounds as models for asphaltenes and studied the emulsion stability and solubility of the models using titration with n-heptane. Despite the large number of studies done on various models for asphaltenes, there are still lots of ambiguity in asphaltene behavior.

Asphaltenes contain a large number of molecules which are very different in structure; therefore modeling asphaltenes using one model compound is not very practical. In a study by Jaffe et al.<sup>40</sup>, there were 125 core structures found in petroleum fractions boiling up through five condensed aromatic ring structures. These structures are shown in Figure 4. Based on these structures, one can make

the vacuum residua molecules by using single core homologous series with longer side chains or using multi-core molecules using the same series.

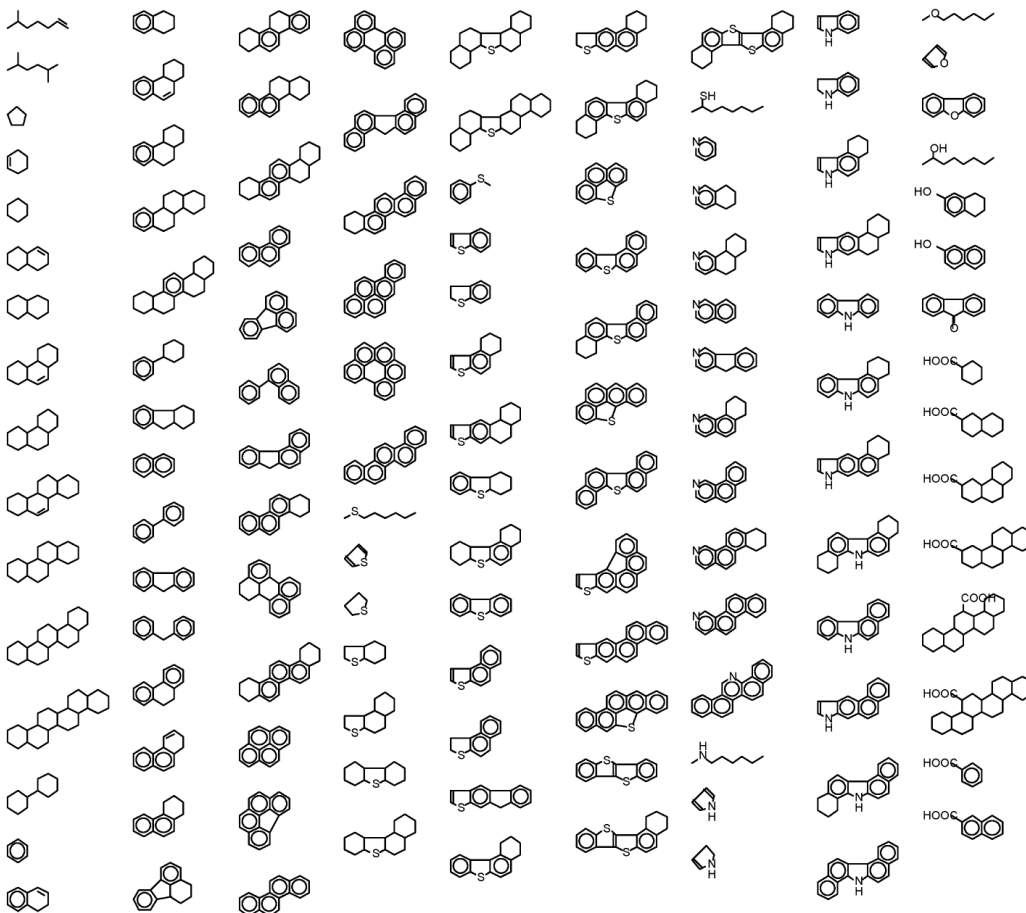


**Figure 4. 125 common core structures in petroleum fractions boiling up through five condensed aromatic ring structures (Taken from reference 40).**

The aggregation behaviour of asphaltene is another subject that attracts a large amount of research. Kawanaka et al.<sup>41</sup> used a colloidal model to present the aggregation behaviour of asphaltene. They suggested that resins are the reason for asphaltene stabilization and keeping them suspended in oil. In their study, they concluded that resins are adsorbed on the asphaltene surface and cause the asphaltene to be stabilized as a result of the repulsion between resins that adsorb on asphaltene surface and resins in the solution. Figure 5 represents this behaviour. Therefore, asphaltene stability is dependent on the amount of resins adsorbed on the surface.

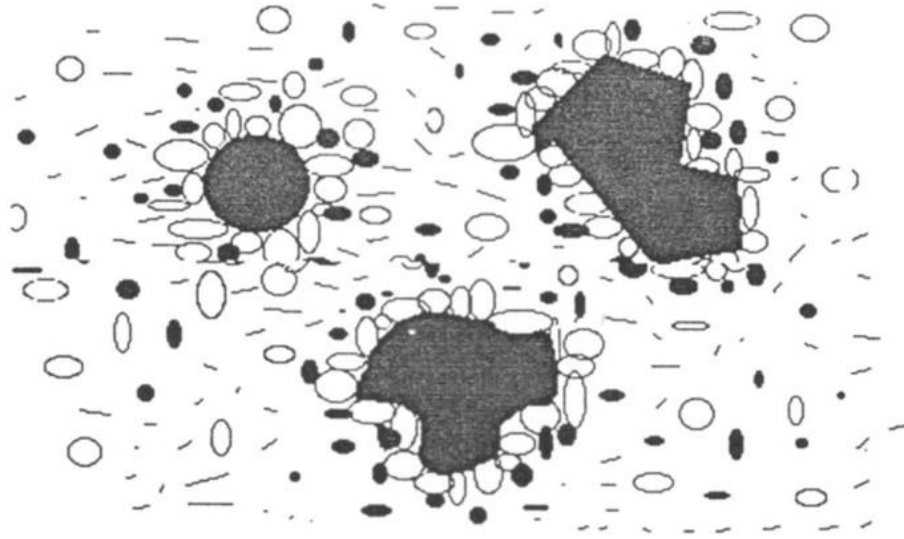


**Figure 5.** ○ resin molecules, ● aromatic molecules, — oil molecules, ■ asphaltene particles. Resins are adsorbed on the asphaltene surface and cause the asphaltenes to be stabilized due to the repulsion between resins that adsorbed on asphaltene surface and resins in the solution (Taken from reference <sup>41</sup>).

Agrawala and Yarranton<sup>42</sup> used a different model to explain the aggregation behaviour of asphaltene. They suggested that the behaviour can be represented in the same way as linear polymerization. In this model, asphaltenes have single or multiple active sites and resins have single active sites. Therefore, asphaltenes can act as a propagator and resin can act as a terminator. This model is shown in Figure 6.

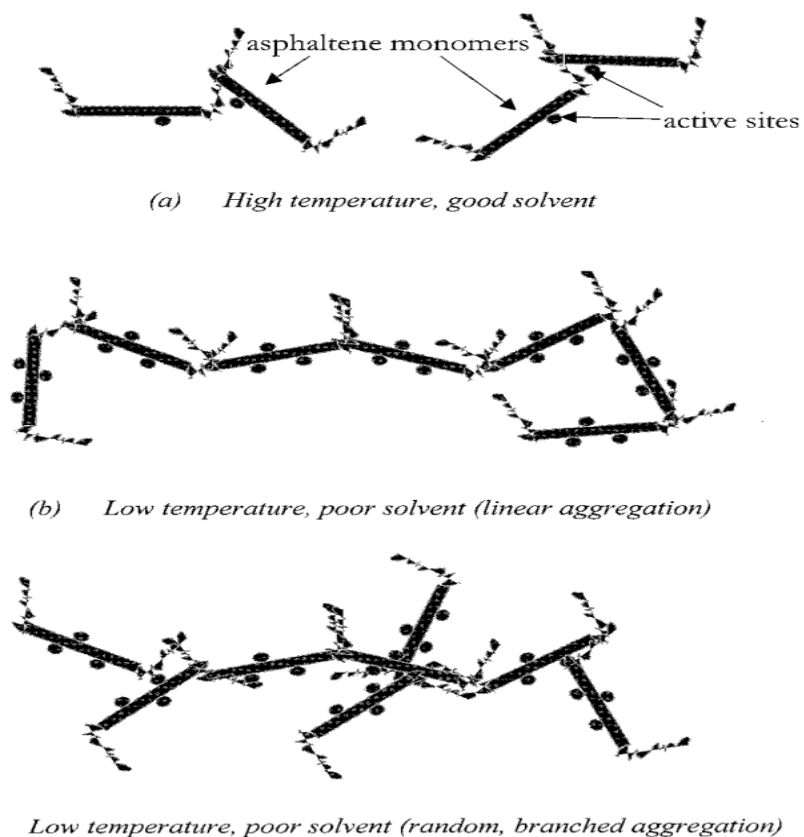


**Figure 6. Polymer-like aggregates of asphaltenes. In this model, asphaltenes have single or multiple active sites and act as propagators and resins have single active sites and act as terminators (Taken from reference 42).**

Recently, Gray and his coworkers<sup>43</sup> suggested a supramolecular assembly model, (Figure 7) which is a new paradigm-combining cooperative binding by acid-base interactions, hydrogen bonding, metal coordination complexes, cycloalkyl and alkyl groups to form the hydrophobic pockets and aromatic pi-pi stacking. This model simulates the aggregation behavior of asphaltene in organic solvents.

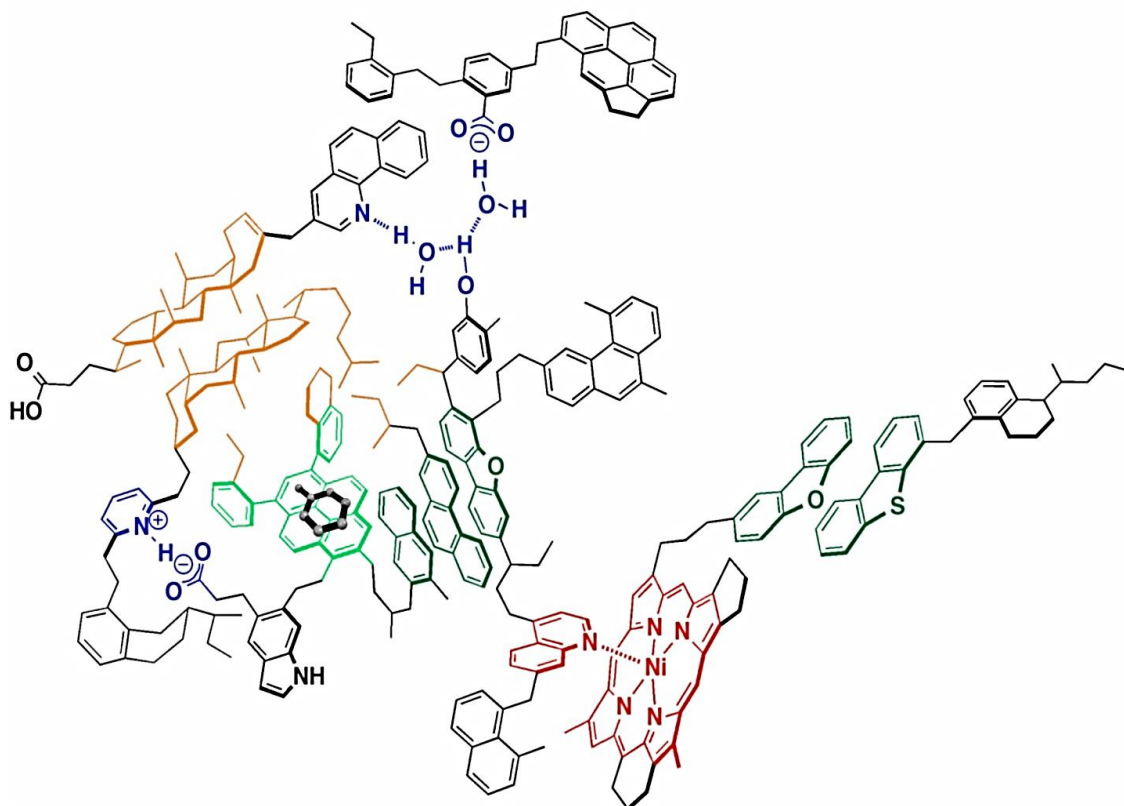


**Figure 7.** Schematic representation of a supramolecular assembly. Molecular interactions are: acid-base interactions and hydrogen bonding (blue), metal coordination complexes (red), hydrophobic pockets (orange) and aromatic pi-pi stacking (green) (Taken from reference 43).

### 1.2.7. Electrical Charge of Asphaltenes

Electrodeposition was the first technique to demonstrate the possible electrical charge of asphaltene aggregates. Katz and Beu<sup>44</sup> as well as Preckshot et al.<sup>45</sup> found positive electrode to be covered with a black material, and the negative electrode to be clean, showing that asphaltene particles were negatively charged, whereas Lichaa and Herrera<sup>46</sup> observed a positive charge on asphaltenes precipitated with olive oil from Venezuelan crudes. Over the years using the

electrodeposition method, it was confirmed that the charge is dependent on the media in which asphaltene is dissolved.

Recently, in order to quantify the charge on asphaltenes, the electrical conductivity<sup>47</sup>, zeta potential<sup>48</sup> and electrokinetic properties<sup>49</sup> of asphaltene sample were measured. The magnitude and sign of the zeta potential of asphaltenes in aqueous solutions can be changed upon the addition of cationic and anionic surfactants<sup>48</sup>, changing the pH of the aqueous medium<sup>48</sup> and composition of the solvent<sup>50</sup>. Asphaltenes from different sources, found to be charged in aqueous mediums such as water or water-oil interface<sup>51</sup>. For example, in aqueous solutions, the electrophoretic mobility (or zeta potential) of asphaltenes is negative above pH 4, however it is positive in nitromethane<sup>49</sup> and toluene<sup>52</sup>. In addition to aqueous solutions, asphaltenes may be charged in organic solvents such as toluene<sup>51</sup>.

### **1.2.8. Summary**

As indicated previously, asphaltenes do not have a precise chemical definition. Their definitions are based upon solubility characteristics. They are soluble in aromatic hydrocarbons such as toluene or benzene, however, they are insoluble in saturated hydrocarbons. Figure 8 shows a general summary of asphaltenes' properties.

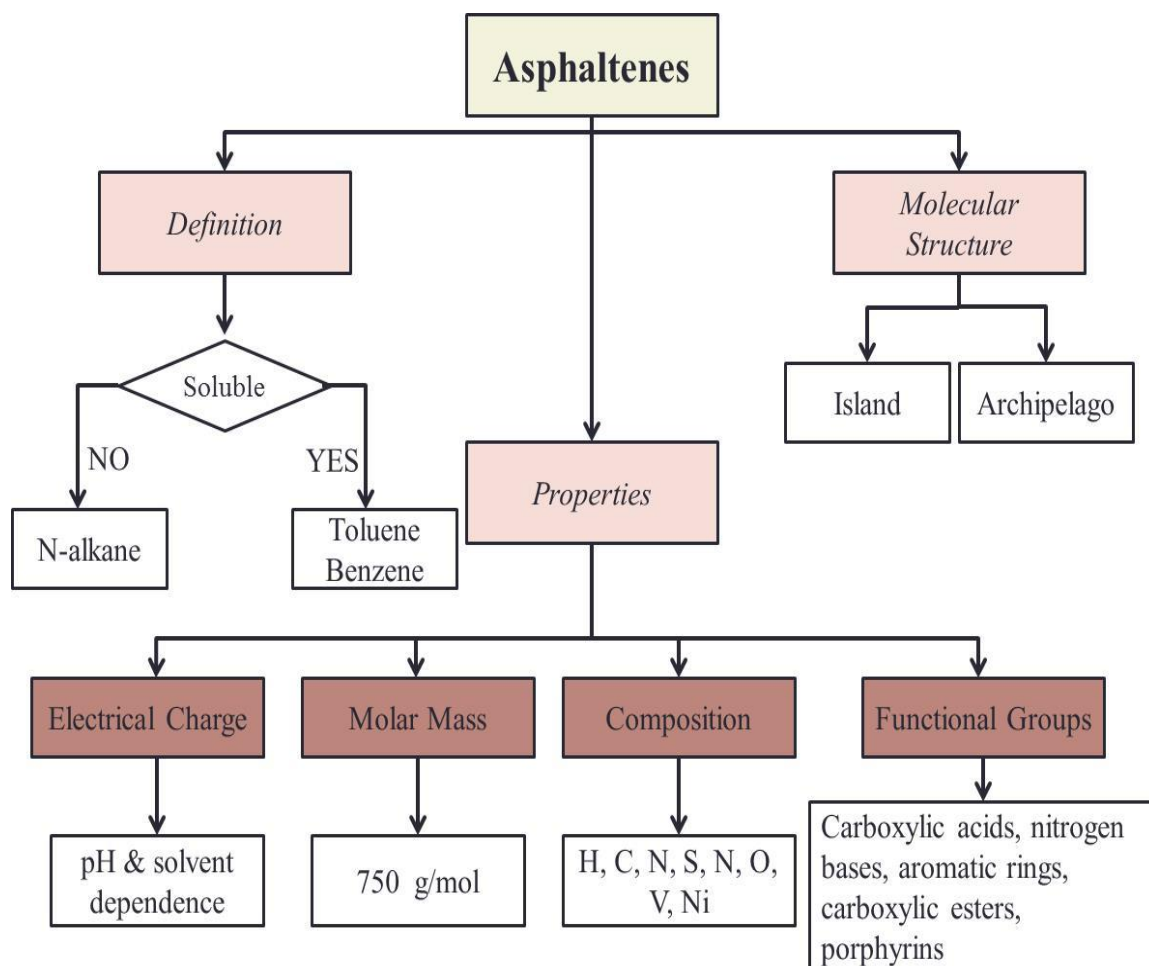


**Figure 8. Summarized asphaltenes' properties.**

### 1.2.9. Thesis Outline

This thesis is arranged in four chapters. The first chapter provides a general introduction to asphaltenes. The challenges in oil sands industry as a result of the presence of asphaltene in bitumen are also discussed.

The second chapter deals with the modification of asphaltenes' surface properties using self-assembled monolayers (SAM) in order to change the wettability and affect the adsorption of asphaltene molecules onto surfaces. It is important to

understand the adsorption of asphaltene on different substrates because of its aggregation and subsequent flocculation characteristics. This chapter also contains results from the adsorption of asphaltenes on self-assembled monolayers of dodecanethiol investigated by FT-IR and ellipsometry.

The third chapter deals with the geometrical and morphological characterization of asphaltene aggregation behavior. In order to understand the dynamics and morphology of asphaltene aggregates, we investigated the variations of topography, adhesion and contact potential differences of asphaltenes aggregates as a function of temperature. The samples for AFM investigation were prepared by evaporating an asphaltenes-toluene solution in ambient conditions.

Based on experimental results obtained, potential future research directions are proposed in the fourth chapter. They include modification of surfaces using self-assembled monolayers for preventing the adsorption of asphaltenes on surfaces as well as investigating the physical and chemical properties of asphaltene aggregates using improved scanning probe techniques.

## Chapter 2

### **Adsorption of Asphaltenes on Self-Assembled Monolayers of Dodecanethiol Accessed by FT-IR and Ellipsometry**

Asphaltenes can be adsorbed on solid surfaces as colloidal aggregates. Alboudwarej and co-workers<sup>53</sup> showed that asphaltenes have a high affinity to interact with hydrophilic metallic surfaces. They concluded that the amount of asphaltenes adsorbed on surfaces decreased in the following order: stainless steel (304L) > iron > alumina. Since the asphaltene fraction consists of polar molecules having amphiphilic characteristics<sup>54</sup>, they can adhere to surfaces through functional groups containing sulfur, nitrogen and oxygen<sup>55</sup>. As a result, adsorption and deposition of these molecules on surfaces create numerous problems for heavy oil recovery and upgrading.

Asphaltene adsorption on surfaces and reservoir rocks limits the extraction of heavy oils from reservoirs by changing the wettability of the surface. This increases maintenance costs and they are responsible for reservoir damage, catalyst deactivation during crude oil processing, equipment fouling and pipelines plugging in oil production and processing facilities<sup>43,56-59</sup>. For example, Dickkian and Seay<sup>59</sup> have shown that asphaltene precipitation and subsequent carbonization is a major cause of refinery heat exchanger fouling. Figure 9 shows asphaltene depositions in a pipeline. As a result of the difficulty that asphaltenes cause during processing in industry, the elucidation of the asphaltene's structure has become increasingly important.

The adsorption of asphaltenes onto solid substrates has been characterized by using different techniques such as atomic force microscopy (AFM)<sup>60</sup>, contact angle measurements<sup>61,62</sup>, UV-Vis spectroscopy<sup>55</sup>, ellipsometry<sup>63</sup>, fourier transform infrared spectroscopy (FT-IR)<sup>64</sup>, etc. In addition to the dependence of asphaltene

adsorption on the surfaces which were mentioned before, the mechanism of adsorption on solid surfaces also depends on the existence of resins and the characteristics of asphaltenic solutions, including the type of asphaltene and its concentration as well as the quality of the solvent.

As a result of the surface active materials in resins, they can also adsorb on the surface and fill the available spaces for adsorption of asphaltenes<sup>53</sup>. Akhlaq et al. monitored the adsorption of asphaltenes from different solvents with diverse polarities, which are toluene, tetrahydrofuran, n-heptane-toluene mixture and chloroform, using contact angle measurements. The contact angle increased when the solvent polarity decreased<sup>62</sup>. Alboudwarej et al.<sup>53</sup> also reported that asphaltenes dissolved in mixtures of n-heptane and toluene adsorbed to a higher extent relative to the adsorption in the toluene solution.

The source of asphaltene is another important factor which affects adsorption of asphaltenes on surfaces since samples from different places do not have the same chemical species. This causes different chemical bonds between the surface and the asphaltenes. Ekholm and co-workers<sup>65</sup> investigated the effect of the solution concentration on the adsorption of asphaltene onto a gold substrate. They concluded that asphaltene adsorption from toluene solution increased as concentration increased.



**Figure 9. Asphaltene deposition in a pipeline.**

The degree of the hydrophobicity of the surfaces can affect the amount of asphaltenes adsorption on the substrates as well. Asphaltenes interaction with the surfaces can be induced by modifying the surface by Self-Assembled Monolayers (SAMs)<sup>66</sup>. SAMs are hydrophobic closely packed monomolecular films formed by the spontaneous adsorption of an active surfactant on a solid surface. More details about SAMs are given in the next part.

Hannisdal et al.<sup>67</sup> studied the asphaltenes adsorption on pure silicon wafer and chemically modified particles. All particles were exposed to asphaltenes/toluene solutions for 24 h. They analysed the toluene solutions for remaining asphaltenes and concluded that hydrophilic particles had adsorbed more asphaltenes than the hydrophobic ones. Cohen and coworkers<sup>66,68</sup> has studied asphaltenes adsorption on silicon substrates modified with monolayer of alkyltrichlorosilanes with different number of carbon atoms and also with mixed monolayer of aliphatic and aromatic trichlorosilanes by means of spectroscopic ellipsometry, contact angle (CA) measurements, and near-edge x-ray absorption fine structure (NEXAFS) spectroscopy. They concluded that asphaltenes adsorption does not correlate with the SAM chemical composition and decreased with an increase in the number of carbon atoms of monolayer.

## 2.1. Self-Assembly Monolayer (SAM)

Self-assembled monolayers (SAMs) are hydrophobic ordered molecular assemblies formed by the spontaneous adsorption of an active substrate on a solid surface<sup>69</sup>. Organosilicon compounds (generally referred to as “silanes”) and organosulfur compounds (generally referred to as “thiols”) are the two most commonly used molecules for production of self-assembled monolayers. These assemblies are formed with the interaction of an active group and the solid surface and used as a means for friction reduction and corrosion prevention<sup>70</sup>. Thiols coordinate very strongly to noble metals such as gold and Ag; however, organosilicon compounds need the hydroxyl groups on the substrate to form a bond<sup>71</sup>. Alkanethiols on gold substrate are widely used since gold is chemically inert and its surface is easy to clean.

Alkanethiols are a class of organic molecules that have a sulfur atom at one end and alkyl chain as back bone that form well-ordered monolayers on the gold substrate<sup>69</sup>. Dodecanethiol used in this project is liquid at room temperature and a simple alkane chain with an S-H as head group attached to a 12 carbon alkane. The diagram of the chemical structure of dodecanethiol is illustrated in Figure 10.

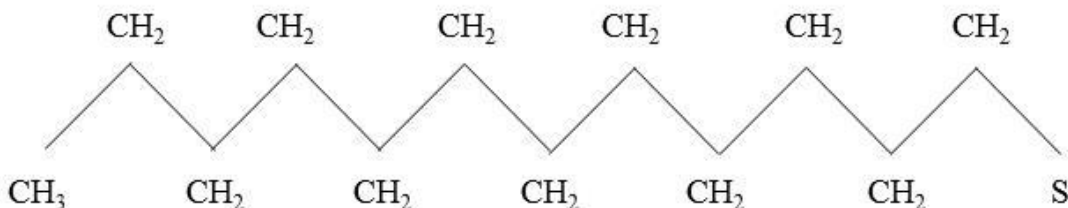


**Figure 10. Chemical structure of dodecanethiol.**

In this research, the growth of self-assembled monolayer from dodecanethiol onto gold substrate has been studied using FT-IR spectroscopy and ellipsometry. Figure 11 is the schematic of two idealized structures for organized self-assemble

monolayer. a) closed-packed arrangement of alkyl chain and sulfur head groups oriented normal to the solid surface, b) closed-packed arrangement of alkyl chain and sulfur head groups oriented at an angle  $\varphi$  from the surface<sup>72</sup>.

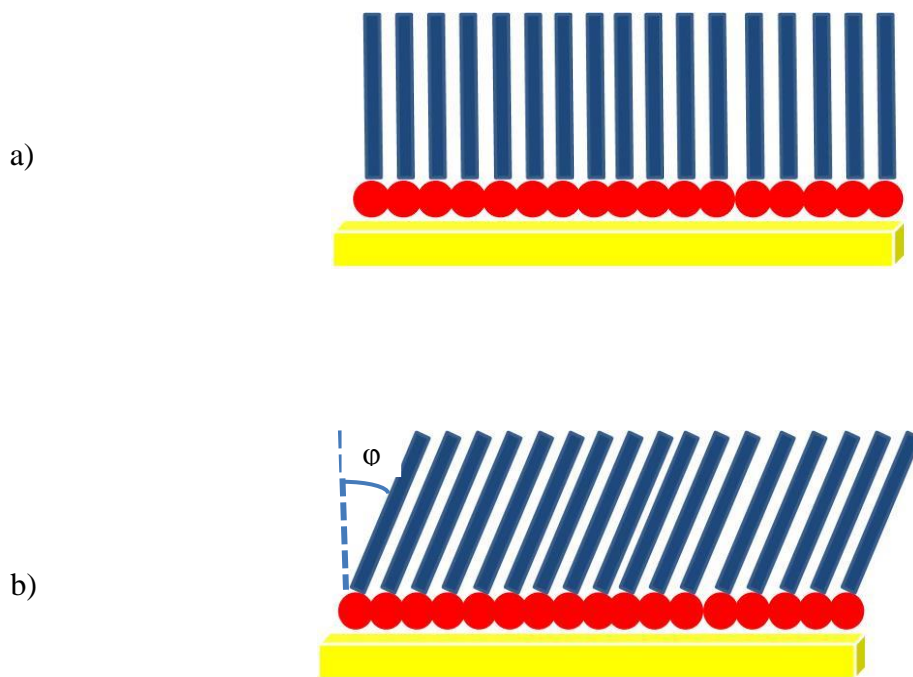


**Figure 11. Schematic of two structural models of self-assembly: a) closed-packed arrangement of alkyl chain and sulfur head groups oriented normal to the solid surface, b) closed-packed arrangement of alkyl chain and sulfur head groups oriented at an angle  $\varphi$  from the surface. The yellow substrate, red circles and blue bars correspond to gold, sulfur head groups and alkane chains, respectively.**

In this study, we tried to create hydrophobic surface by creating a dodecanethiol self-assembled monolayer (SAM) on gold coated borofloat glass substrate. In this chapter, we investigate the adsorption of asphaltene on substrates coated with hydrophobic monolayer and gold-coated samples. It is known from literature that asphaltene does not adsorb on hydrophobic surfaces<sup>66,68</sup>, hence as a control we formed self-assembled monolayer on the gold-coated borofloat substrates.

## 2.2. Experimental Methods

### 2.2.1. Materials and Chemicals

Dodecanethiol  $\geq 98\%$  was bought from Sigmaaldrich (Canada), HPLC grade heptane and toluene were obtained from FisherScientific (Canada). These chemicals were used as received. Borofloat substrates were obtained from Nanofab (Univ. of Alberta, Edmonton). Industrial asphaltene samples used in this work were obtained from OrCrude. It was precipitated by pentane from Athabasca bitumen, Nexen plant, and was about 50% heptane-insoluble materials.

### 2.2.2. Asphaltenes Preparation

Detail compositions of asphaltenes use in this study are showed in the table below<sup>73</sup>.

**Table 2. Composition of the asphaltene sample (Taken from reference 73).**

	Heptane-insoluble (wt%)	Toluene-insoluble (ppm)	V content (ppm)	Ni content (ppm)
<b>Asphaltene</b>	50	<0.05	580	230

Pure asphaltene was obtained by mixing it with n-heptane in a 1:40 (g:ml) followed by sonication for 30 min and then stirring for 24 hr. The mixture was vacuum filtered using a 0.22  $\mu\text{m}$  filter paper at room temperature and atmospheric pressure. The filter cake was rinsed with n-heptane until the effluent was colorless. Finally rinsed asphaltenes samples were left in a fume hood for 2 days to ensure a complete evaporation of n-heptane and stored at room temperature, Figure 12.



**Figure 12. Asphaltenes sample.**

### **2.2.3. Solution preparation**

Asphaltenes solution (0.5% w/w) was prepared by dissolving appropriate amounts of dried asphaltene in HPLC-grade toluene. The mixture was stirred and then sonicated for 10 minutes to ensure a complete dissolution. Figure 13 illustrates the asphaltene/toluene solution.

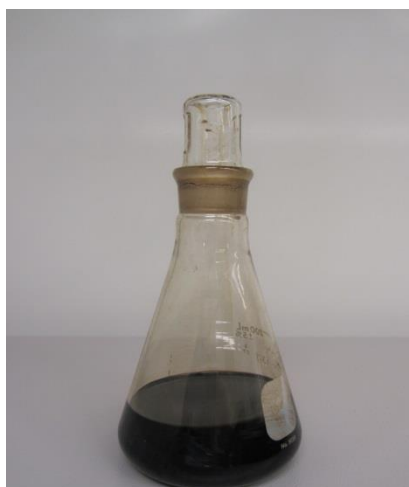


**Figure 13. Asphaltene/toluene solution.**

#### 2.2.4. Sample preparation

Borofloat substrates were cleaned by rinsing with a piranha solution (1:3 H<sub>2</sub>O<sub>2</sub>/H<sub>2</sub>SO<sub>4</sub>) to remove organics, followed by water and nitrogen drying. Glass substrates were sputter-coated under a vacuum ( $1.3 \times 10^{-6}$  torr) with titanium as an adhesion layer for 84 s followed by gold for 1050 s. The sputtering system was equipped with argon gas at a pressure of 7 mtorr. All films employed a 10 nm thick Ti and 100 nm thick gold. Finally, all substrates were cut into small pieces approximately ( $1 \times 1$  cm<sup>2</sup>). Prior to dodecanethiol exposure, gold substrates were cleaned with piranha solution and drying with nitrogen gas to minimize the presence of organic contamination before dodecanethiol deposition.

There are two different methods for growing monolayers of alkanethiols on the substrate. First and widely used method is using solution. Another method of preparation is using vapor deposition in ultra-high vacuum. In this study, we used the first method and used ethanol solution for SAM growing. Gold-coated substrates were immersed in a clean container containing 1 mM dodecanethiol in absolute ethanol, wrapped with parafilm and stored for 24 hours at room temperature in a dark area.

The schematic of the preparation of dodecanethiol on gold-coated substrate is shown in Figure 14. The growing of SAMs on the surfaces progresses in three steps. In the first step, a low density “striped” phase is formed. In this phase, alkane chains lying flat, head-to-head or head-to-tail arrangement, on the gold surface (Figure 14 a). This is followed by an “intermediate” stage and surface is covered with more alkanethiol molecules (Figure 14 b). Finally, in the “standing up” phase, a closed-pack oriented monolayer is formed on the surface (Figure 14 c)<sup>74</sup>.

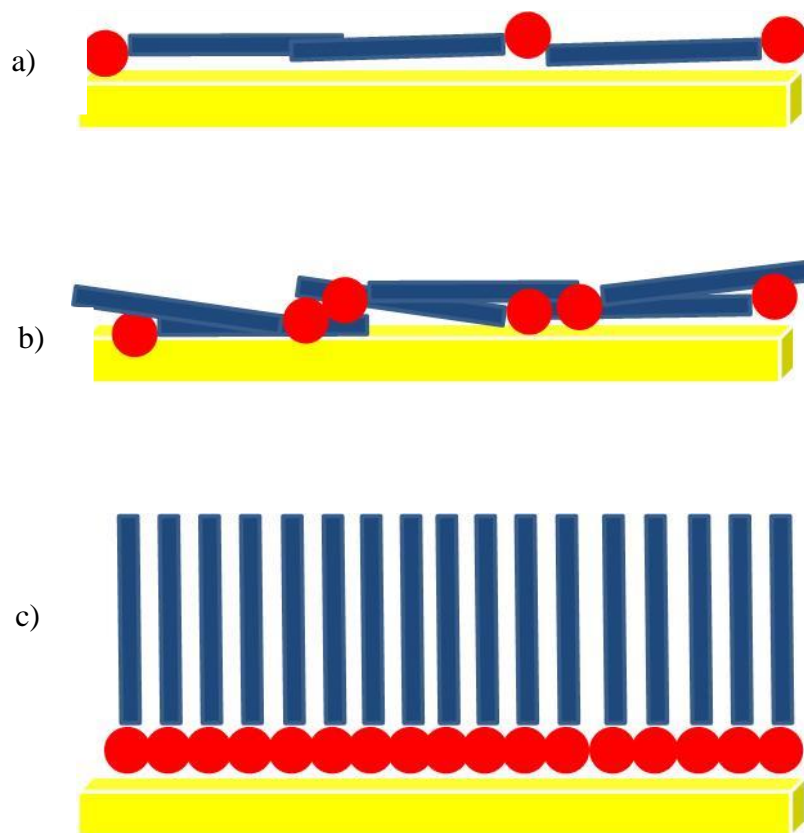


**Figure 14. Schematic of SAM preparation. The yellow substrate, red circles and blue bars correspond to gold, sulfur head groups and alkane chains, respectively. In the first stage (a), a low density “striped” phase is formed. This is followed by an “intermediate” stage (b) and finally, in the “standing up” phase (c), a closed-pack oriented monolayer is formed on the surface.**

In many SAM schemes found in literature, self-assembly monolayers on gold substrate are considered as ideal monolayers, however there are several types of defects at the molecular level on the surface that cause the idea of closed-packed configuration far from real. Figure 15 shows different types of surface defects<sup>75</sup>.

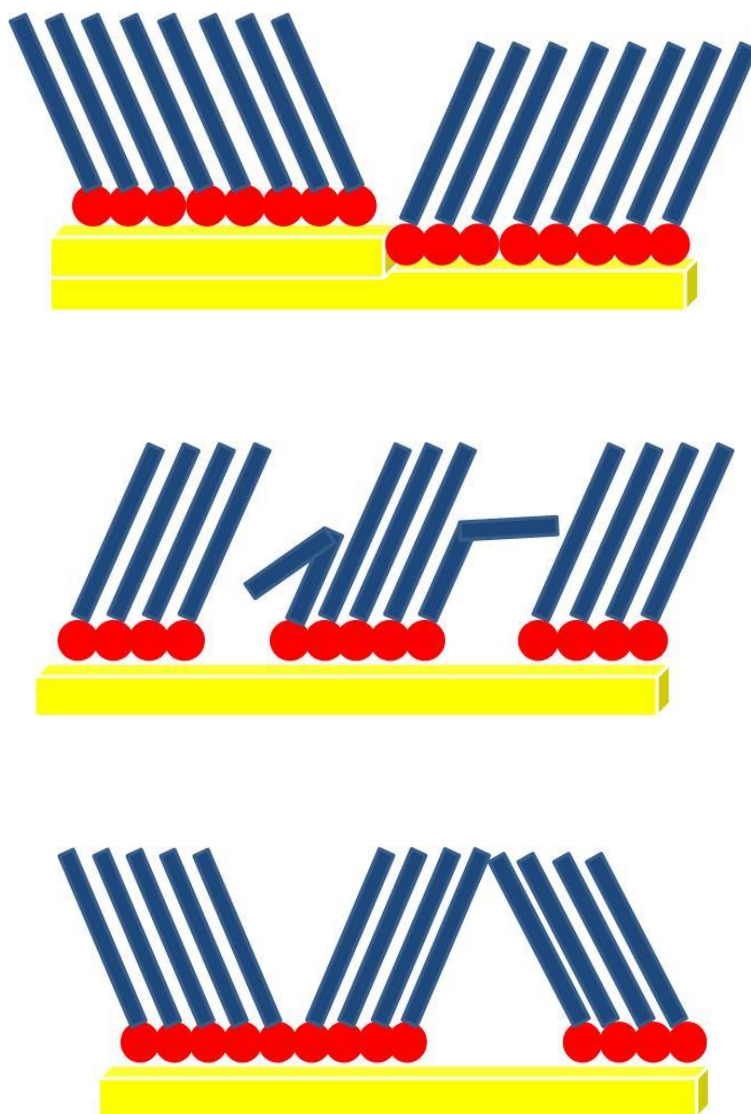


**Figure 15. Different types of surface defects. The yellow substrate, red circles and blue bars correspond to gold, sulfur head groups and alkane chains, respectively.**

After 24 hours, the substrates were removed from depositing solution, quickly rinsed with absolute ethanol to remove physisorbed over layers and dried with nitrogen gas. Finally, FT-IR spectroscopy and ellipsometry were used to confirm the growing of self-assembled monolayer on the gold substrate. Once the SAM was formed on the gold substrates and confirmed by FT-IR spectroscopy and ellipsometry, they were immersed in asphaltenes solution for 12 hours at room temperature and placed in a dark area. The samples were then rinsed with toluene, and then dried with nitrogen gas. The adsorption of asphaltene on the

SAM-coated substrates is monitored by characterizing the functional groups, and measuring the film thickness by using FT-IR spectroscopy and ellipsometry, respectively.

### **2.2.5. FT-IR Measurements**

Infrared radiation is the part of the electromagnetic spectrum between the visible and microwave regions. Fourier Transform Infra-Red (FT-IR) spectroscopy is an excellent tool for molecular recognition. FTIR technique has been routinely used to detect the presence of molecules on the substrate by monitoring the absorbance of infrared radiation at frequencies that correspond to the vibration of the specific functional group bonds in the molecule<sup>76</sup>. It is a sensitive tool that can detect very thin molecular layers on solid surfaces. In this study, FT-IR spectra were recorded on a Nicolet Nexus 670 FT-IR spectrometer in the absorbance mode with a DTGS detector and a nitrogen-purged sample chamber. Each spectrum resulted from the accumulation of 1000 scans with a spectral resolution of 4  $\text{cm}^{-1}$ , and incident angle of 70°. The FT-IR spectra of the background substrate were performed using a clean gold surface reference spectrum.

#### **2.2.5.1. Dodecanethiol on Gold Substrate**

Infrared spectra of the samples were recorded in the range 1000 and 3500  $\text{cm}^{-1}$ . A considerable part of the infrared work in this research was in the range of between 2800-3000  $\text{cm}^{-1}$ ; this range has been used with characteristic adsorption bands from C-H stretching in methyl and methylene groups. Figure 16 shows the IR absorbance spectra of dodecanethiol on gold substrate in the range of 2800-3000  $\text{cm}^{-1}$ . The spectra of SAM-coated sample clearly show symmetric and asymmetric stretching vibrations of the  $\text{CH}_2$  groups at about 2850  $\text{cm}^{-1}$  and 2921  $\text{cm}^{-1}$ , respectively, and  $\text{CH}_3$  symmetric aliphatic stretching mode at about 2877  $\text{cm}^{-1}$  and 2933  $\text{cm}^{-1}$ . The wavenumber of 2964  $\text{cm}^{-1}$  is assigned to the  $\text{CH}_3$  asymmetric in-

plane (ip) aliphatic stretching mode. Table 3 shows the peak positions of dodecanethiol which was absorbed on gold substrate. The spectra were obtained at a spectral resolution of  $4\text{ cm}^{-1}$  using 1000 scans per spectrum. Four samples have been prepared and the FTIR measurements have been done on all of them. For all of the samples the same peaks were observed.

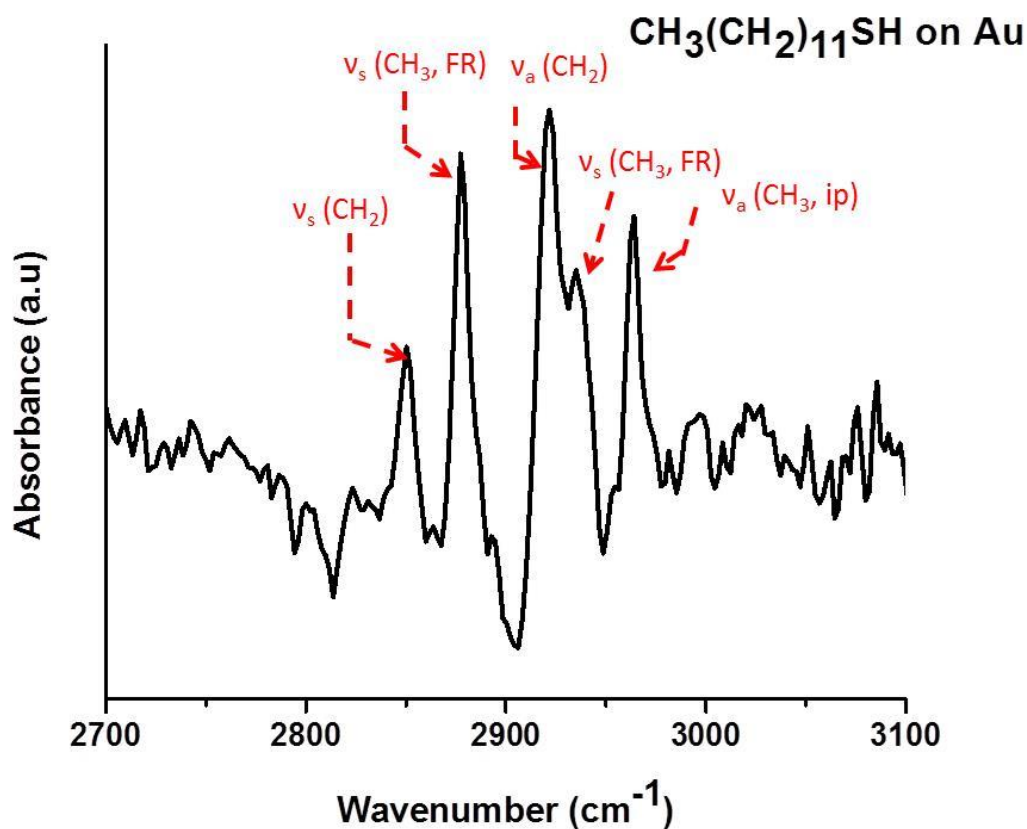


Figure 16. FTIR absorption spectrum peaks of dodecanethiol on gold substrate. Peaks between  $2800\text{ cm}^{-1}$  and  $3000\text{ cm}^{-1}$  correspond to absorption by CH<sub>3</sub> and CH<sub>2</sub> bonds of alkane chain.

**Table 3. Peak position for CH<sub>3</sub>(CH<sub>2</sub>)<sub>11</sub>SH**

Structural groups	C-H stretching mode	Peak positions for CH <sub>3</sub> (CH <sub>2</sub> ) <sub>11</sub> SH adsorbed on gold substrate
-CH <sub>2</sub> -	$\nu_a$	2921
	$\nu_s$	2850
CH <sub>3</sub> -	$\nu_a$ (ip)	2964
	$\nu_s$ (FR)	2877
	$\nu_s$ (FR)	2933

Similar spectra have been reported for several thiols groups on gold<sup>77</sup>. The results provide clear evidence for creation of dodecanethiol monolayer on the surface.

### 2.2.5.2. Asphaltenes on Gold Substrate

In order to examine asphaltene adsorption on the bare gold substrates, FT-IR spectroscopy was used. The presence of asphaltene was successfully demonstrated with FT-IR results and shown in Figure 17.

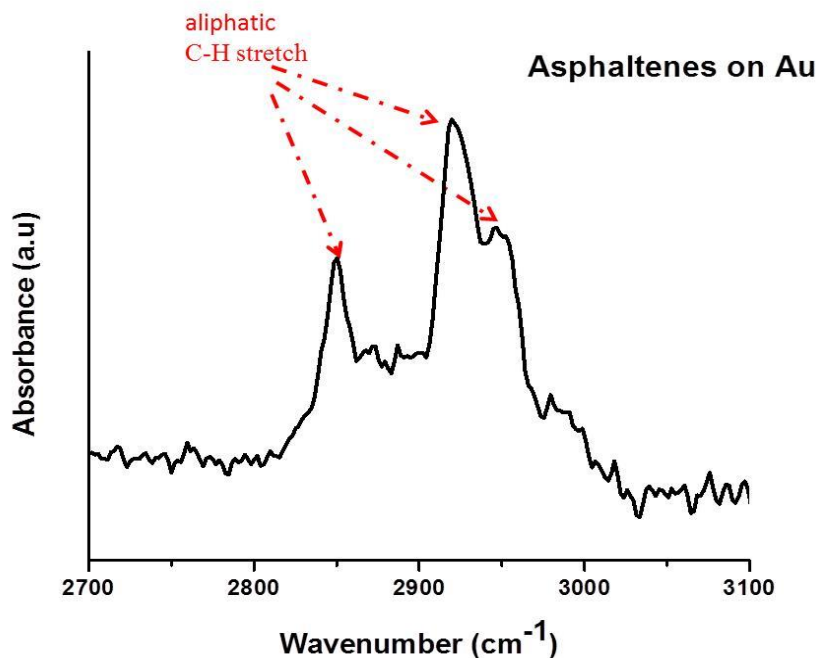


**Figure 17. FTIR spectra of the asphaltenes on gold substrate.**

The FTIR spectra of the asphaltenes on gold substrate are presented in Figure 17. These peaks are related to corresponding symmetric and asymmetric stretching frequencies of methyl and methylene groups. It was understood from FT-IR analysis that asphaltenes deposited on the surface. Numerous FT-IR spectroscopy studies have been conducted to study the composition of asphaltenes<sup>78-81</sup> and confirm the peaks in Figure 17.

### **2.2.5.3. Asphaltenes on SAM-Coated Gold Substrate**

FT-IR spectra are also performed after immersing SAM-coated substrates in asphaltenes solution for 12 h at room temperature. This result is presented in Figure 18.

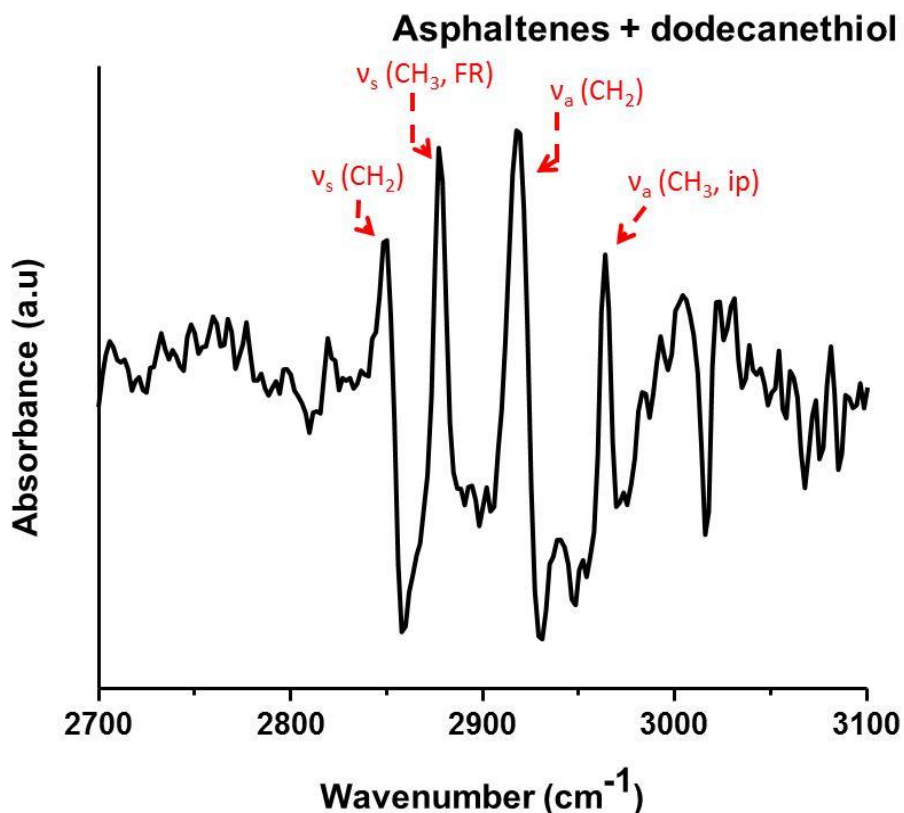


Figure 18. FT-IR absorption spectrum peaks of asphaltene on SAM-coated substrate. Peaks between  $2800 \text{ cm}^{-1}$  and  $3000 \text{ cm}^{-1}$  correspond to absorption by  $\text{CH}_3$  and  $\text{CH}_2$  bonds of alkane chain.

A comparison between the FT-IR spectra of dodecanethiol on Au and asphaltenes on SAM shows that the absorbance for SAM peaks have not changed when asphaltenes was added to the sample. Therefore, it can be concluded that SAM inhibits the adsorption of asphaltenes from its surface.

### 2.2.6. Ellipsometry Measurements

Measuring the thickness of self-assembled monolayer and asphaltenes on the gold substrate is a part of our research. Ellipsometry was performed to measure the thickness of films on samples that were prepared identically and in parallel with those used in the FT-IR spectroscopy. Ellipsometry is an optical technique that has been widely used for film thickness determination. It measures the change in

the polarized light reflected from the sample surface<sup>82</sup>. Figure 19 shows the schematic of ellipsometry. The measurements are performed by sending a known polarization beam of light from a polarizer towards the sample and output polarization is determined by a rotating analyzer.

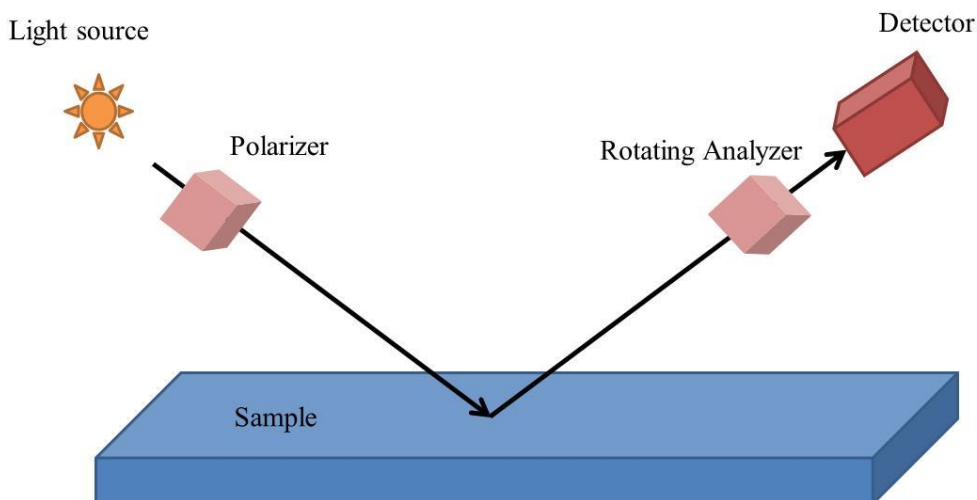


**Figure 19. Schematic of ellipsometry experiment.**

Porter et al.<sup>72</sup> employed null-point ellipsometer to measure the thickness of n-alkyl thiols with different carbon atom numbers. They concluded that the structure of the longer-chain assemblies (number of methylene groups in the chain  $\geq 9$ ) is more ordered than that of the short-chain assemblies. Henry et al.<sup>63</sup> used ellipsometry to measure the thickness of asphaltene film adsorbed from the toluene solution in different concentration on a glass substrate after 24 and 48 h. The thickness of the asphaltene film measured was found to be in the 20-298 nm range for 24 h and after that it was found to be increased.

In the present research, film thickness of bare SAM and SAM-asphaltenes was determined with Sopra GESP-5 ellipsometer. Four different areas in the film surface in three samples were scanned to obtain film thickness uniformity at  $\lambda=450$  nm, index of refraction  $n=1.5$ , and incident angle  $75^\circ$ . WINELLI software

was used in order to calculate the thickness of the layers. The ellipsometry results are presented in Table 4.

**Table 4. Film thickness (in Å) on gold-coated substrate as determined by ellipsometry.**

	SAM thickness (Å)	(SAM+Asp.) thickness (Å)	Asp. thickness (Å) on gold (without SAM)
Average	$14.3 \pm 1.1$	$15.6 \pm 0.9$	$28 \pm 1.7$

Porter et al.<sup>72</sup> used ellipsometry to measure the thickness of dodecanethiol on the gold substrate and reported the average thickness approximately 18 Å.

Figure 20 shows the schematic of asphaltene adsorption on the gold-coated and SAM-coated substrate.

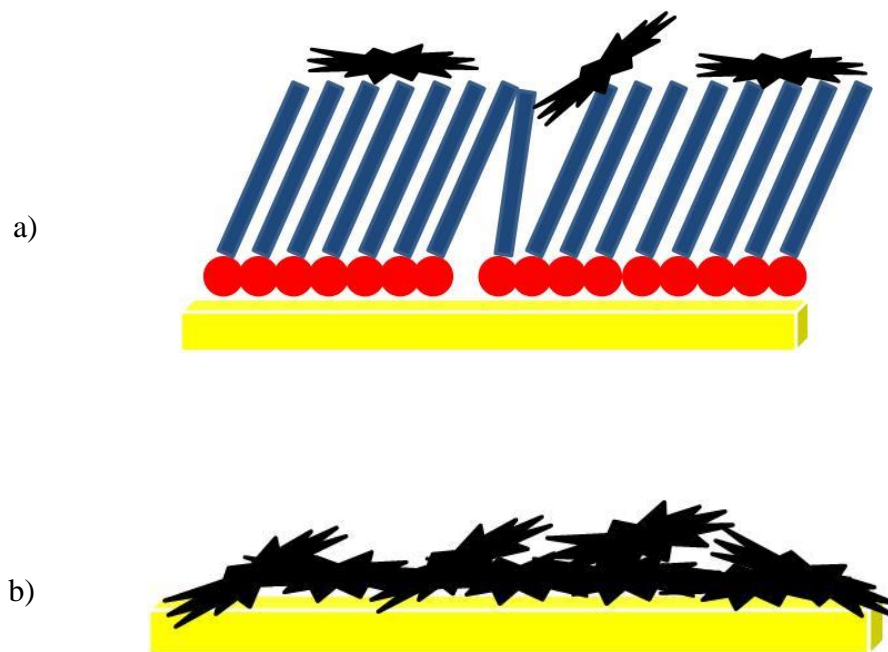


**Figure 20. Schematic of asphaltene adsorbed on a) dodecanethiol modified and b) gold coated substrate. The yellow substrate, red circles and blue bars correspond to gold, sulfur head groups and alkane chains, respectively. Asphaltene aggregates are shown in black.**

The thicknesses in Table 4 are reported as the average of three different locations of three samples with the error given as standard deviation. This thickness of asphaltenes could be related to the multilayer adsorption of asphaltenes aggregates or the asphaltene molecule. As it was mentioned before, the aggregation of asphaltene molecules in toluene initiates at concentration as low as 50-100 ppm<sup>17,19,20</sup>. As a result, the adsorption of asphaltenes on the solid surface will be the aggregates. It was concluded from the results in Table 4 that the adsorbed amount of asphaltenes decreases significantly on dodecanethiol modified gold substrate.

## Chapter 3

### AFM Measurements

#### 3.1. An Overview on Atomic Force Microscopy (AFM)

The atomic force microscopy (AFM) is a powerful tool that belongs to a series of scanning probe microscopes invented in the 1980s by Binnig et al.<sup>83,84</sup>. AFM is capable of producing high resolution images yielding information about surface topography and characteristics of surfaces at the nano-scale dimension.

The AFM machine consists of a sharp tip mounted at the end of a flexible cantilever as a probe, a piezoelectric element to bring the sample towards and away from the surface, laser diode, and position-sensitive photodiode detector (PSD), as illustrated in Figure 21. In order to measure the cantilever deflection and producing an image a laser diode and PSD are employed. The laser is reflected off of the top of the tip and any deflection of the cantilever, changes the position of the laser and the photodiode monitors these changes. These changes are sending to the feedback controller where the data is processed and projected as an image on the computer. In the AFM, the sample is scanned by the tip and by measuring the tip and cantilever deflection versus its position on the sample, a topographic image of the sample is obtained. Force between the tip and the substrate can also be measured as well by monitoring the deflection of the cantilever<sup>83</sup>. Atomic force microscopic can be operated in different environments such as air, liquid or vacuum.

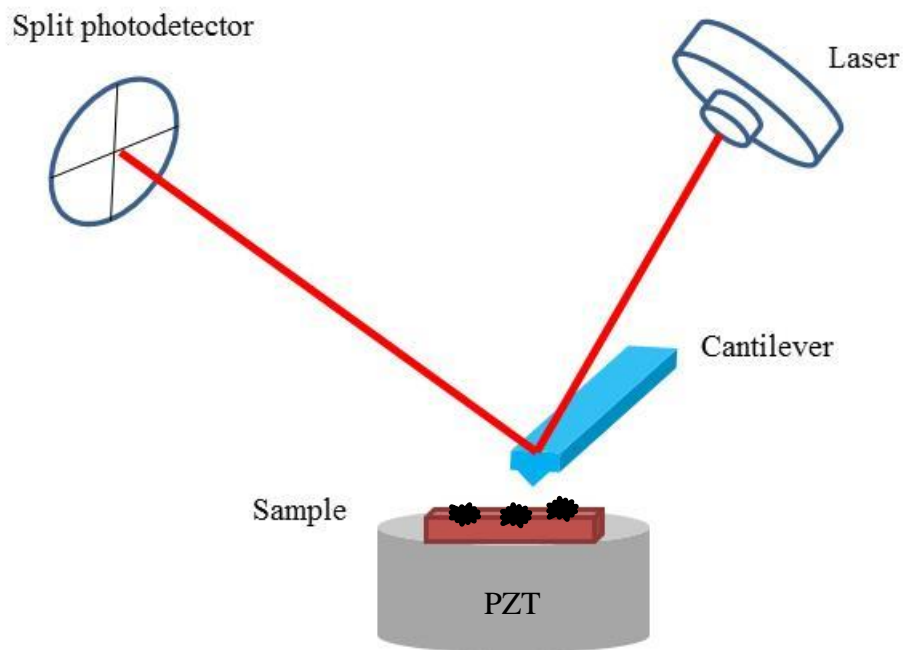


**Figure 21. Schematics of an atomic force microscopy. It consists of a sharp tip mounted at the end of a flexible cantilever, a piezoelectric element, laser diode, and photodetector.**

AFM can operate in two different modes: Tapping mode and contact mode. In tapping mode, the probe oscillates at its resonance frequency in order to scan the surface. In contact mode, the tip moves in continuous contact with the surface either at constant force or constant height. Unlike the contact mode which is associated with high shear forces, tapping mode is suitable for soft samples and the damage to the sample surface is minimized because the tip contacts the surface intermittently without damaging it.

In order to investigate surface characteristics, diverse imaging techniques such as atomic force microscopy (AFM), scanning electron microscopy (SEM) and transmission electron microscopy (TEM) are used. SEM and TEM provide a 2-dimensional surface profile, however AFM provides a 3-dimensional image of a sample, so that it is possible to measure the height of the particles quantitatively. SEM has a somewhat lower resolution to AFM. TEM and SEM usually operate in

a vacuum and require a conductive sample so samples are coated with a metallic layer that would change or damage the sample, however sample viewed by AFM do not require any special treatments. Most AFM modes can work perfectly well in room temperature air or even a liquid environment, however an electron microscope needs a vacuum environment for proper operation.

Understanding the dynamics and morphology of asphaltenes aggregates have attracted massive research attention for several decades. In this section, a brief review is presented on the few prior studies about the asphaltenes microstructure and the effect of temperature on the morphology of the asphaltenes nano-aggregates. In a study by Sourty et al.<sup>85</sup>, dependence of thickness on concentration and spin coating at different rotation speed was investigated by AFM. Different concentrations of binders in toluene (binders are refinery residues from deep thermal conversion processes) were deposited on cleaned glass substrate and rotated at constant speed ranging from 500-5000 r.p.m for 120 s. They concluded that thickness increases with concentration and decreasing rotation speed.

Asphaltenes domains formed from the two different binders showed differences in their growth behavior. They<sup>85</sup> also investigated the effect of annealing on the structure of binder thin films with two concentrations of 5% and 50% in toluene with AFM. Thin films on glass substrates were heated up to 60 °C in stage I and to 120 °C in stage II, and after each stage, the samples were cooled down to 25 °C (Figure 22).

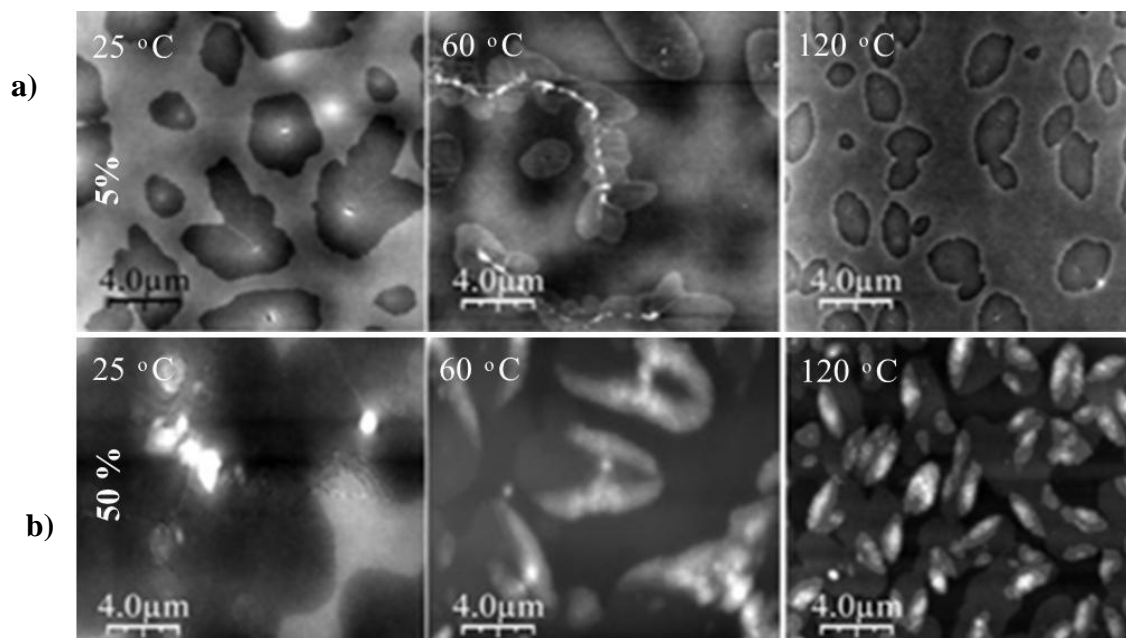


**Figure 22. Topography images of sample 1, a) 5% (top), b) 50% (bottom). Thin films were heated up to 60 °C in stage I and to 120 °C in stage II, and after each stage, the samples were cooled down to 25 °C (Taken from reference <sup>85</sup>).**

In sample one, which originated from high-sulphur crude and contain about 25% asphaltenes as shown in Figure 22a, after stage I, flower-like domains tend to string together. After stage II, these aggregates were broken. In Figure 22b, high concentration (50%), after stage I (60 °C), the larger aggregates broke down into small ones. After stage II (120 °C), the aggregates decreased in area and strung together. As it observed in Figure 22, after a heat treatment until 60 °C, the low-concentration (5%) sample illustrated further aggregation of asphaltenes.

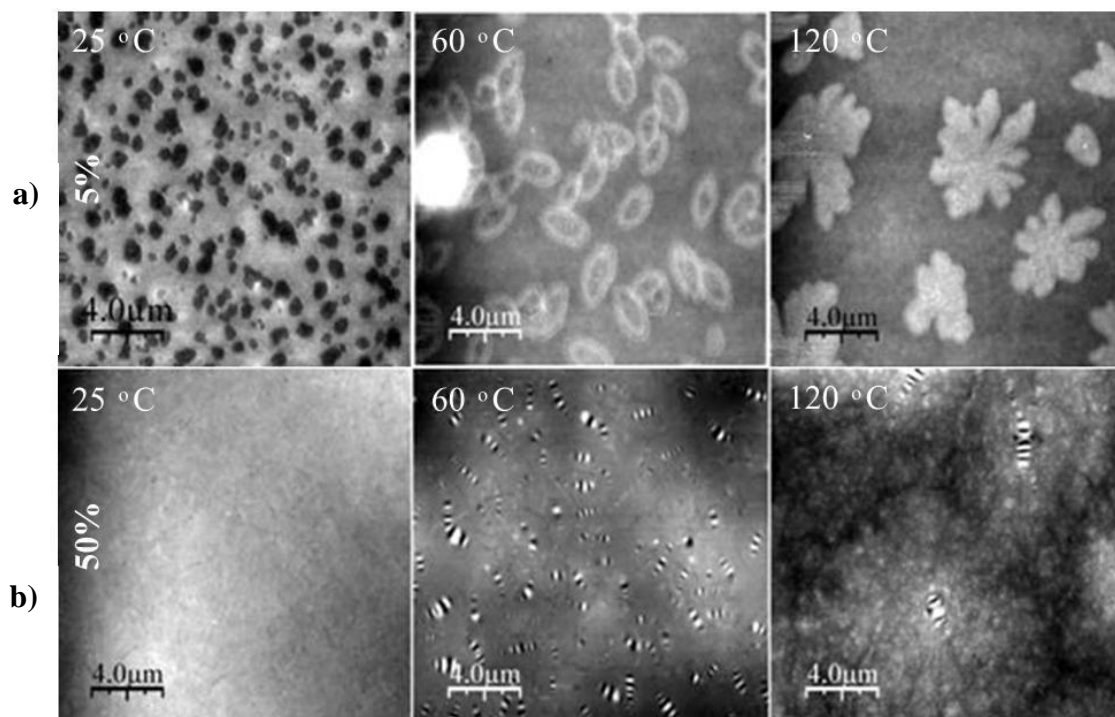


**Figure 23.** Topography images of sample 2, a) 5% (top), b) 50% (bottom) (Taken from reference 85).

As Figure 23 shows, on sample two with low concentration in toluene (5%), after heat treatment until 60 °C, domains increased in size and after stage II in 120 °C, domains fused together and form flower-like shapes. On the concentration of 50% the domains' size increased by increasing temperature. The formation of bee-like wavy fingers at the center of domains is also remarkable.

In another study by Toulhoat et al. 1994<sup>60</sup> asphaltenes aggregation morphology onto cleaved mica sheets as a function of immersion time, and on a comparison of the structures formed by filtered and unfiltered asphaltenes were investigated by AFM. Mica substrates were dipped into toluene solutions containing dissolved asphaltenes and dried. They finally concluded that, an unfiltered asphaltenes solution contains material which is poorly solvated in toluene. Moreover, the adsorption from unfiltered solutions resulted in the flower-like diffusion limited aggregation (DLA) of asphaltenes on mica surface.

In this study, we used an advanced mode of AFM called as Peak Force-Kelvin Probe Force Microscopy (PF-KPFM) which is a combination of frequency modulation KPFM and PF-AFM. It allows quantitative work function measurements at top spatial resolution with higher sensitivity and accuracy.

### 3.2. An Overview on Kelvin Probe Force Microscopy (KPFM)

Kelvin probe force microscopy (KPFM), is an AFM-based technique and has been extensively used for characterizing the electrical properties of materials at nanometer scale. It is a non-contact AFM (NC-AFM) operation mode that measures the contact potential difference (CPD) between a conducting tip and the sample surface. A simple schematic of KPFM is shown in Figure 24. The CPD between the tip and sample is defined as<sup>86</sup>:

$$V_{\text{CPD}} = \frac{\Phi_{\text{tip}} - \Phi_{\text{sample}}}{-e}$$

Where,  $\Phi_{\text{sample}}$  and  $\Phi_{\text{tip}}$  are the work function of the sample and tip, respectively, and  $e$  is the electronic charge. When an AFM tip is brought close to the sample, due to the differences in Fermi energy levels of tip and sample surface, the electrical force is created between them.

In order to measure the work functions of the sample and tip, the mechanical excitation is switched off and both AC voltage ( $V_{\text{AC}}$ ) at the resonance frequency of the cantilever between tip and sample, and DC voltage ( $V_{\text{DC}}$ ) to the tip are applied.  $V_{\text{AC}}$  is applied between tip and sample resulting in an oscillation of cantilever. The oscillation of cantilever is induced by the electrostatic forces. Therefore, by applying DC voltage to the tip, the electrostatic force interaction will be nullified<sup>87</sup>.

In addition to characterizing the topography of the sample surface, single pass KPFM technique is used to simultaneously measure the surface potential

distribution of the surface. In order to measure the surface potential distribution, the tip is scanned over the surface at a small distance between tip and sample surface ( $\sim 5-50\text{nm}$ )<sup>88</sup>.

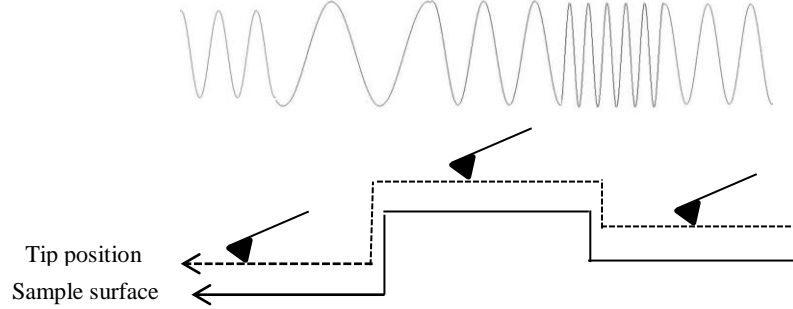


**Figure 24. Schematic depiction of KPFM**

Van der Waals force ( $F_{vdw}$ ), electrostatic force ( $F_{es}$ ) and the force which vibrates the tip ( $F_{vib}$ ) acts on the sample surface and tip. The electrostatic force between the tip and the sample is given by<sup>89</sup>: The surface potential information is derived from the  $F_{es}$ , which is given by<sup>89</sup>

$$F_{es}(z) = \frac{1}{2} \frac{\partial C(z)}{\partial z} V^2, \quad (1)$$

$$V = V_{DC} - V_{CPD} + V_{AC} \cos(2\pi\omega t) \quad (2)$$

Where  $z$  is the direction normal to the sample surface,  $\omega$  is the frequency and  $\frac{\partial C(z)}{\partial z}$  is the capacitance gradient between tip and sample surface.

Substituting equation 2 in 1 gives the expression of the electrostatic force applied to the tip:

$$F_{es}(z, t) = \frac{1}{2} \frac{\partial C(z)}{\partial z} [V_{DC} - V_{CPD} + V_{AC} \cos(2\pi\omega t)]^2 \quad (3)$$

This equation can be divided into three different parts as follows:

$$F_{DC} = \frac{1}{2} \frac{\partial C(z)}{\partial z} [(V_{DC} - V_{CPD})^2 + \frac{1}{2} V_{AC}^2] \quad (4)$$

$$F_{\omega} = \frac{\partial C(z)}{\partial z} (V_{DC} - V_{CPD}) V_{AC} \cos(2\pi\omega t) \quad (5)$$

$$F_{2\omega} = \frac{1}{4} \frac{\partial C(z)}{\partial z} V_{AC}^2 \cos(2 \times 2\pi\omega t). \quad (6)$$

Equation (4) is the static part of electrostatic force and it is difficult to detect. However, equation (5) and (6), the dynamic part, can be detected with a lock-in amplifier to measure the surface potential<sup>70</sup>.

### 3.3. Materials and Methods

Solvents N-heptane and HPLC grade toluene were purchased from Fisher Scientific. Silicon wafers, used as the substrates in our studies, were purchased from NanoFab (University of Alberta, Canada). The two component glue was used to glue the silicon wafers on metal discs for AFM imaging. All the topographical, adhesion and contact potential differences between tip and sample imaging were performed using Peak Force-Kelvin Probe Force Microscopy (PF-KPFM) (Bruker Icon AFM, Santa Barbara, CA). The samples for AFM investigations were prepared by depositing asphaltenes solution onto silicon substrates. Both single-pass mode and lift-mode with a typical scan rate of about 0.7 Hz were used in collecting the AFM images. The PF-KPFM mode was implemented due to its high lateral resolution of contact potential difference and repeatability.

For imaging, PF-tapping mode is used and the instrument operated in air at room temperature. Si<sub>3</sub>N<sub>4</sub> cantilevers coated with Pt/Ir (SCM-PIT, Bruker nanoscience, Santa Barbara, CA) with a nominal resonance frequency of about 75 kHz and spring constant of 2.8 N/m were used. The nominal radius of curvature of tips was around 20 nm.

### **3.3.1. Asphaltenes Preparation**

In this study, we used industrial asphaltene that has 50% heptane-insoluble materials and was precipitated by pentane from Athabasca bitumen. The procedure of asphaltenes precipitation was described in chapter 2.

### **3.3.2. Solution Preparation**

Asphaltenes solution (0.005% w/w) was prepared by dissolving appropriate amounts of dried asphaltenes in HPLC-grade toluene. The mixture was sonicated to ensure a complete dissolution.

### **3.3.3. Depositing of Asphaltenes on SiO<sub>2</sub> Wafer Surface**

Silicon wafers were cut into the small 1cm x 1cm pieces and rinsed by Milli-Q water and ethanol to remove debris from cleaving the sample. The silicon pieces were then dried with nitrogen gas. We used silicon wafer since it is a good thermal gradient and can withstand the heat as compared to mica and gold coated substrates. A drop of diluted asphaltene in toluene solution (0.005 %w/w) was deposited on SiO<sub>2</sub> wafer substrate.

For AFM measurements, two kinds of samples were prepared. In the first one, after dropping asphaltene solution on the silicon wafer, the sample was placed in vacuum oven in 150 °C for about 2 hours. However, in the second one, the asphaltene drop was allowed to evaporate from the surface at room temperature. The two components of glue were mixed with the same ratio and the wafers substrates were glued to the disc and left for 15 min to cure. The sample was then mounted on a heating element installed under AFM probe.

### 3.4. Results and Discussion

For AFM imaging, two methods were used to prepare silicon wafer substrates. The control experiment of silicon substrate was done before dropping asphaltene solution (Figure 25 ).

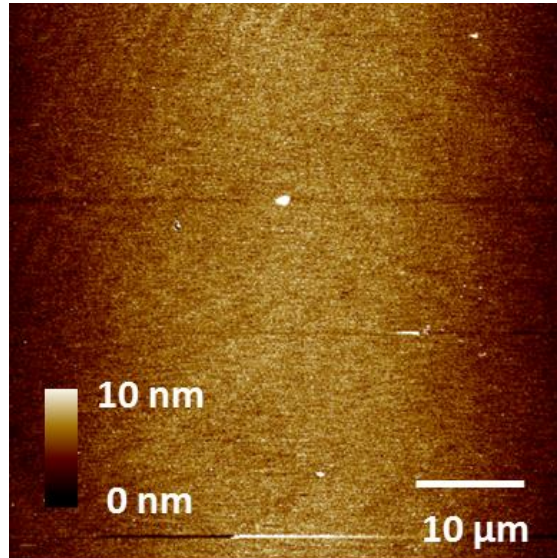


**Figure 25. Control bare SiO<sub>2</sub>**

In the first method, after dropping asphaltene/toluene solution on the SiO<sub>2</sub> wafer, the sample was heated in a vacuum oven in 150 °C for about 2 hours in order to evaporate toluene. The asphaltene aggregates in a peculiar pattern as seen in the optical image in Figure 26. It should be noted that the streaks of asphaltenes are caused by their self-assembly and no external medium was used to cause this pattern. Figure 27, A, B, C and D represent the topography images of specified sections A, B, C and D in Figure 26, respectively. It is obvious that depending on the location, the asphaltenes morphology was different.

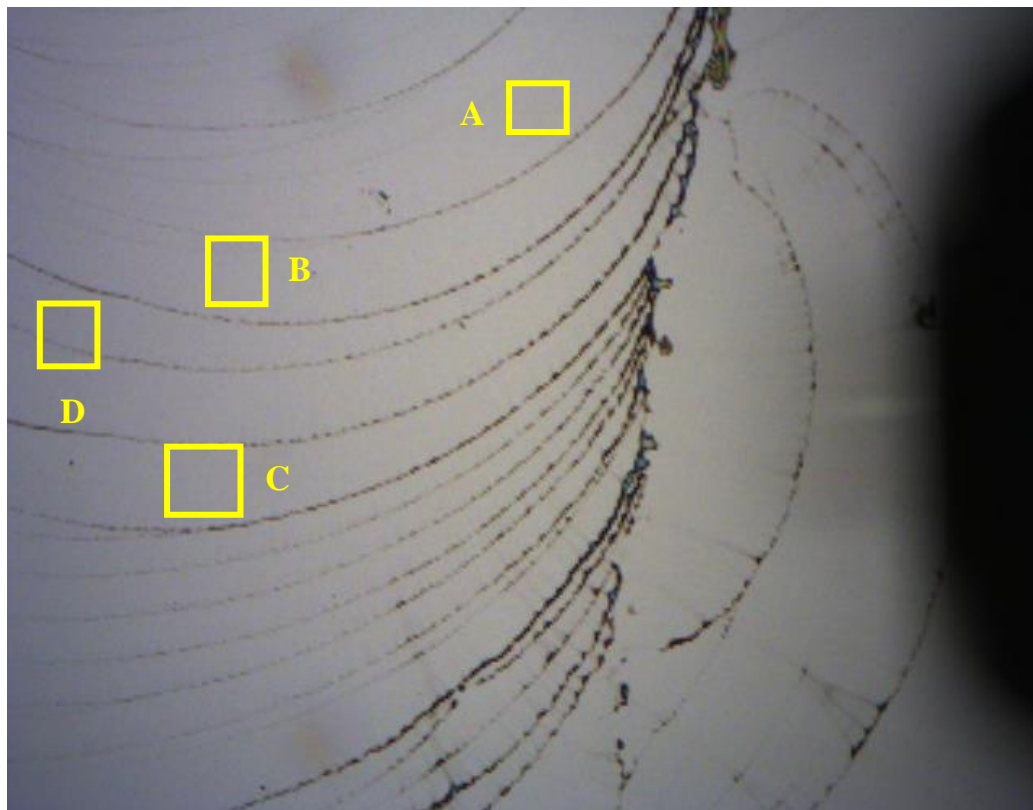


**Figure 26.** The optical image of asphaltene aggregates in a peculiar pattern. The sample was heated in vacuum oven in 150 °C for about 2 hours.

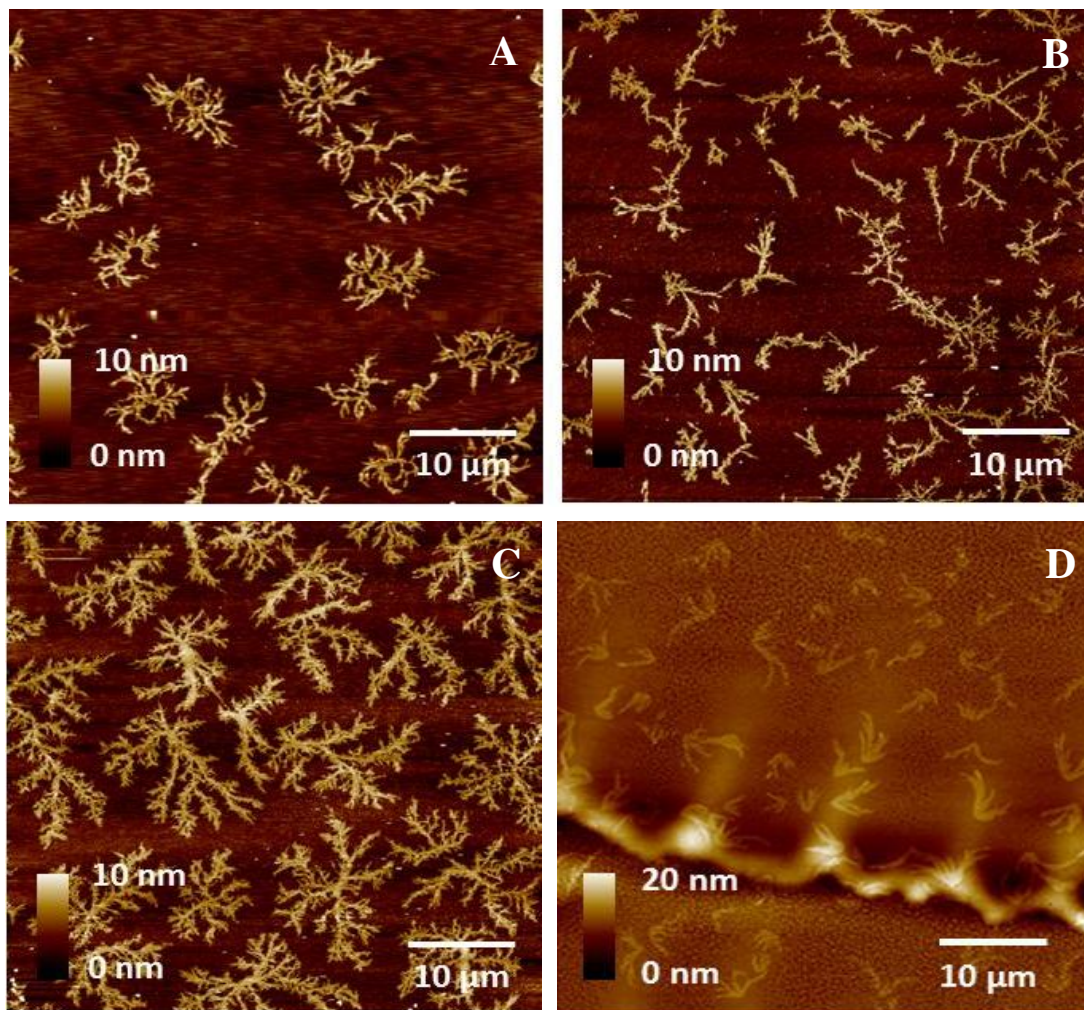


**Figure 27.** Topography of asphaltene on different locations of silicon wafer substrate, heated up to 150 °C for 2 hours.

In another experiment, we were interested not just in the topography of these structures but also in the dynamics of asphaltene aggregates as a function of temperature. We investigated changes in morphology and material properties like adhesion and contact potential difference of the asphaltene nano-aggregates at various temperatures. The fusing of asphaltene domains into large islands at higher temperatures and the corresponding change in its physical properties may help to understand the asphaltene aggregation in oil sands industry. In this experiment, after rinsing silicon wafers with ethanol and drying with nitrogen gas (Figure 28 a), a drop of asphaltene/toluene solution was cast deposited on the

silicon wafer (with native oxide layer (~ 2nm) substrate) (Figure 28 b) and allowed to evaporate at ambient room temperature for 30 minutes to ensure that all the toluene has been evaporated (Figure 28 c). As part of our interest, the effect of annealing on the morphology of the asphaltenes aggregates was investigated. The samples were mounted on the heating element installed just below the AFM tip and a potential bias of 0.5V was applied between tip and sample (Figure 28 d). Thin films of asphaltene aggregates on SiO<sub>2</sub> substrate were heated up to different temperatures. In order to avoid any domain displacement due to the AFM tip raster scan, after setting the heating element to the next higher temperature, the temperature was allowed to stabilize for about 15 min before the AFM scan. This precautionary step assures us that the domain dynamics is purely due to the thermal energy gained by the asphaltene aggregates.

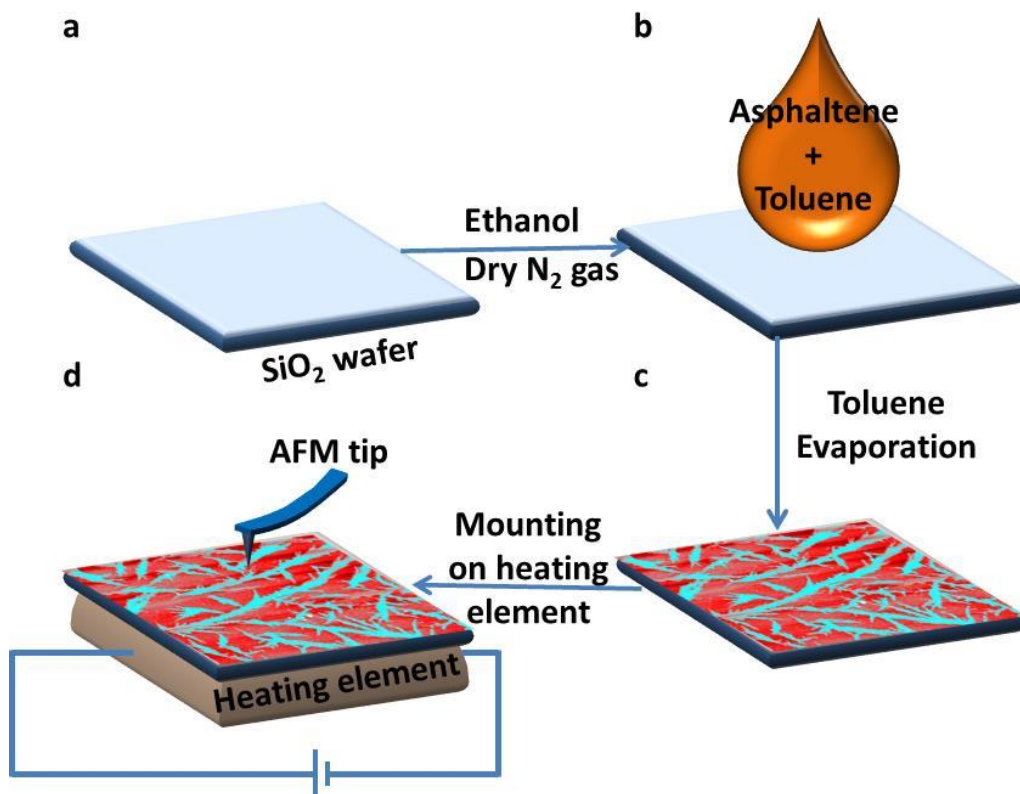


**Figure 28.** (a) Silicon wafers were rinsed with ethanol and dried with N<sub>2</sub> gas, (b) A drop of asphaltenes/toluene solution was cast deposited on the silicon wafers, (c) Toluene was allowed to evaporate at ambient temperature for 30 minutes, (d) The samples were mounted on the heating element installed below the AFM tip.

The topography images of asphaltene at different temperatures of 25, 55, 65 and 80 °C are shown in Figure 29A, B, C and D, respectively. Images were obtained for various samples at different locations and temperatures, but a representative image was presented. In a typical self-assembly of asphaltenes aggregates, the height of aggregates is in the range of nanometer and resembles a micron sized fern-like structure as shown in Figure 29. Asphaltenes are known to form similar structures as observed previously on the glass<sup>85</sup> and mica<sup>60</sup> substrates.

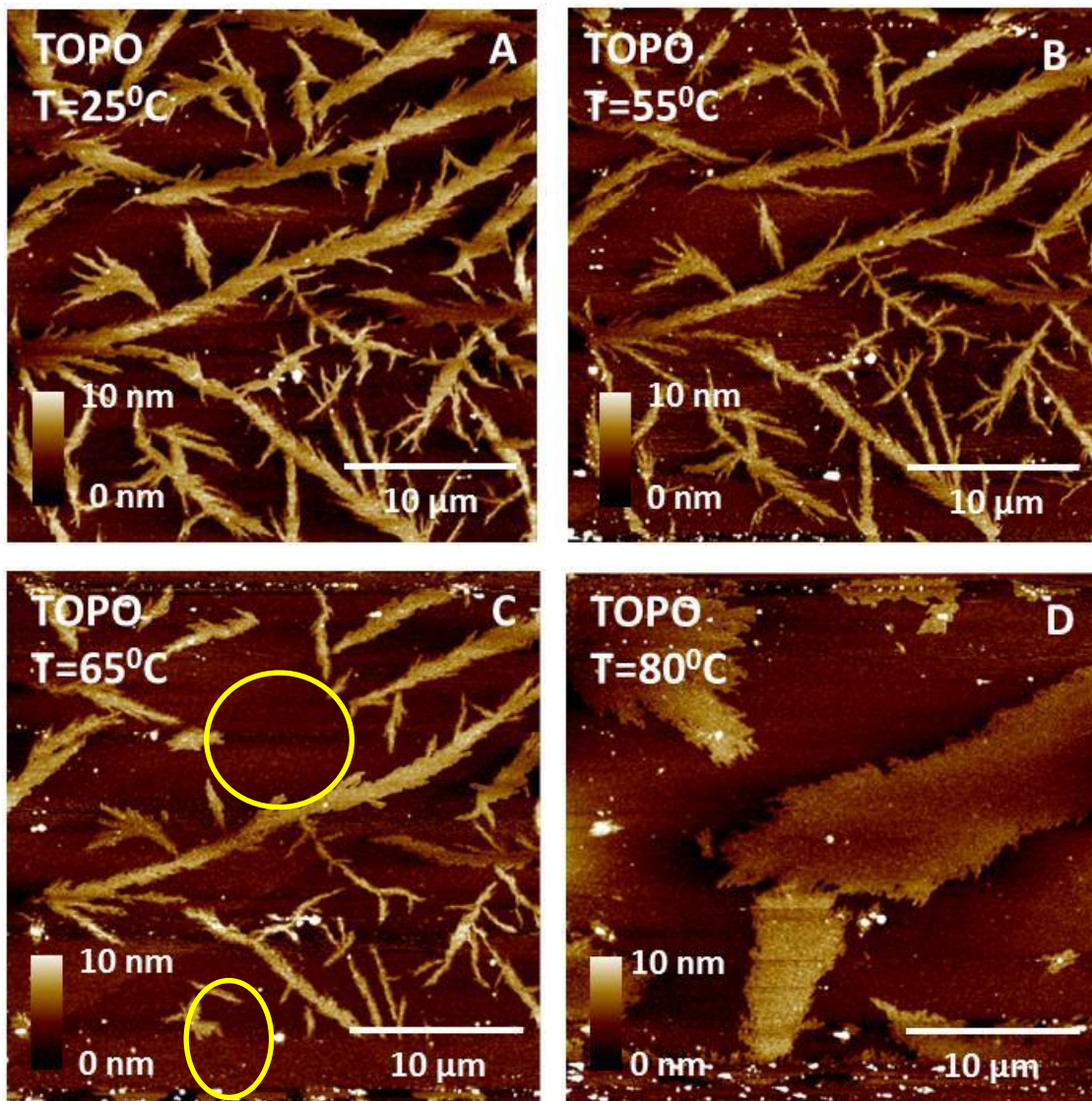


**Figure 29.** Topographic AFM images at different temperatures (A) 25<sup>0</sup>C, (B) 55<sup>0</sup>C, (C) 65<sup>0</sup>C and (D) 80<sup>0</sup>C. A drop of asphaltene solution was cast deposited on the silicon wafer substrate and allowed to evaporate at room temperature.

As seen from topographic images in Figure 29, the self-assembled aggregates are adsorbed in their most thermodynamically stable state at room temperature (25<sup>0</sup>C). The structure of asphaltene aggregates changes by varying the temperature from 25<sup>0</sup>C to 80<sup>0</sup>C. It is observed that as the temperature is increased, the hair-like branched structures coming out from the larger fern-like structures and start to disappear as they gain thermal energy.

As seen in Figure 29A, at approximately 25 °C, the asphaltene aggregates have fern-leaf like structures in which it seems that smaller branches have grown from the larger branches. We find imperceptible variation in the fractal structure of the asphaltene domains for a large range of temperature, from 25 °C to 65 °C. However, morphology of the asphaltene colloidal aggregates changes significantly in a much smaller temperature ranges of 65 °C to 80 °C. Asphaltene aggregates are found to acquire liquid-like mobility and get fused with neighboring aggregates. At this temperature, due to higher thermal energy of smaller branches, they start to disappear. Figure 29C shows that one such domain disappears in the topography image (shown with yellow circles).

Figure 30 represents the height distribution of asphaltene aggregates as a function of temperature. As seen in Figure 30 the height distribution of these fern-like structures decreases from 6.4 nm at 25 °C to 4.4 nm at 60 °C and then somehow become stable at 90 °C.

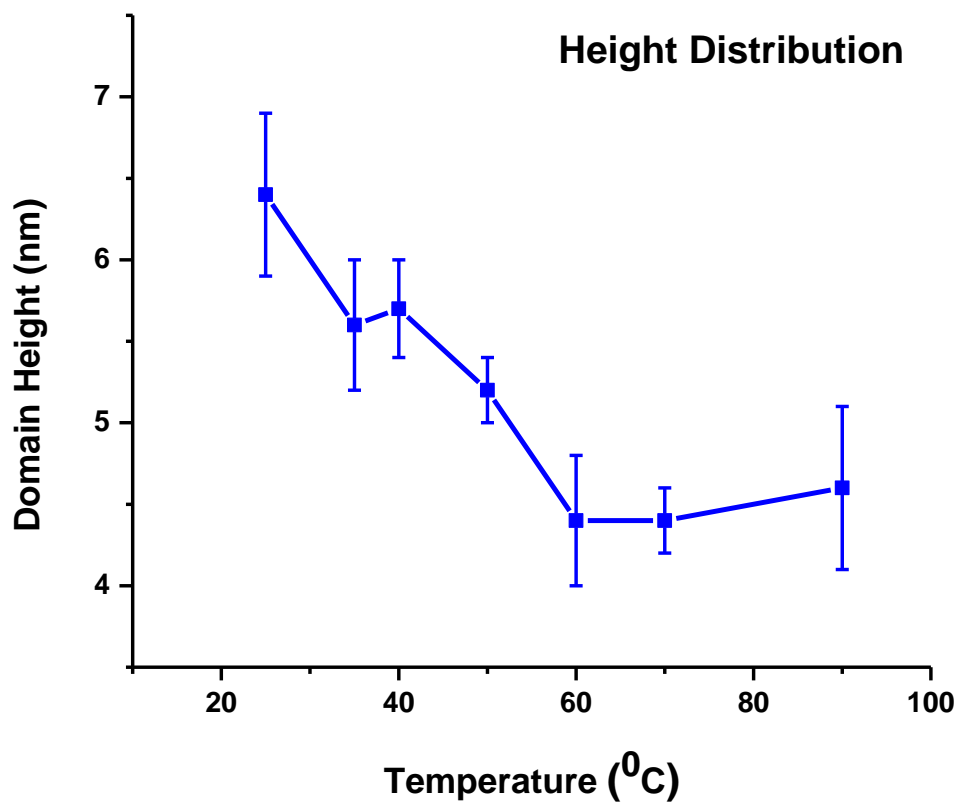


Figure 30. Height distribution of asphaltenes aggregates at various temperatures.

Also, we investigate the adhesion and contact potential difference of these aggregates as a function of temperature. As seen from Figures 31 and 32, not only the structure changes in the topography of self-assembled asphaltenes aggregates in Figure 29, but also the corresponding change in  $V_{CPD}$  and adhesion was detected by increasing the temperature from 25 °C to 80 °C.

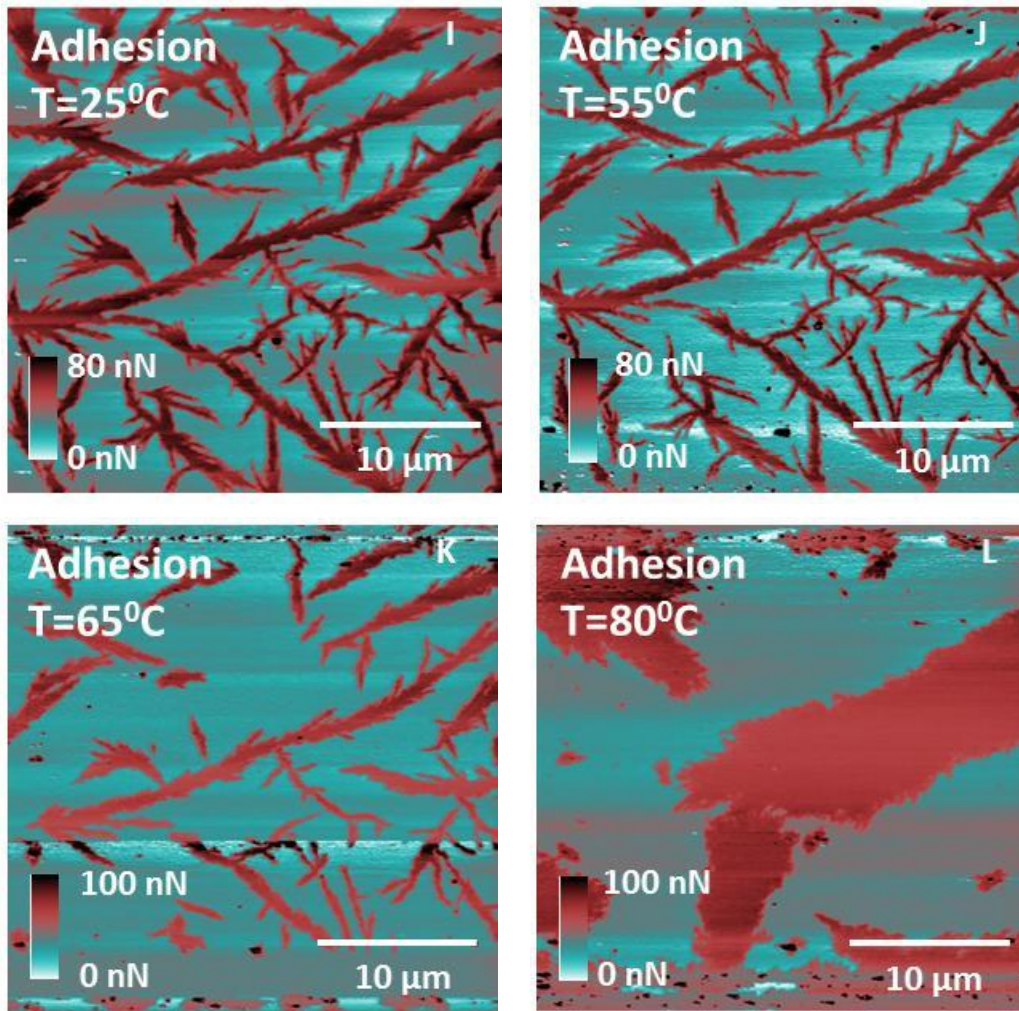


Figure 31. The adhesion at temperatures (I) 25°C, (J) 55°C, (K) 65°C and (L) 80°C.

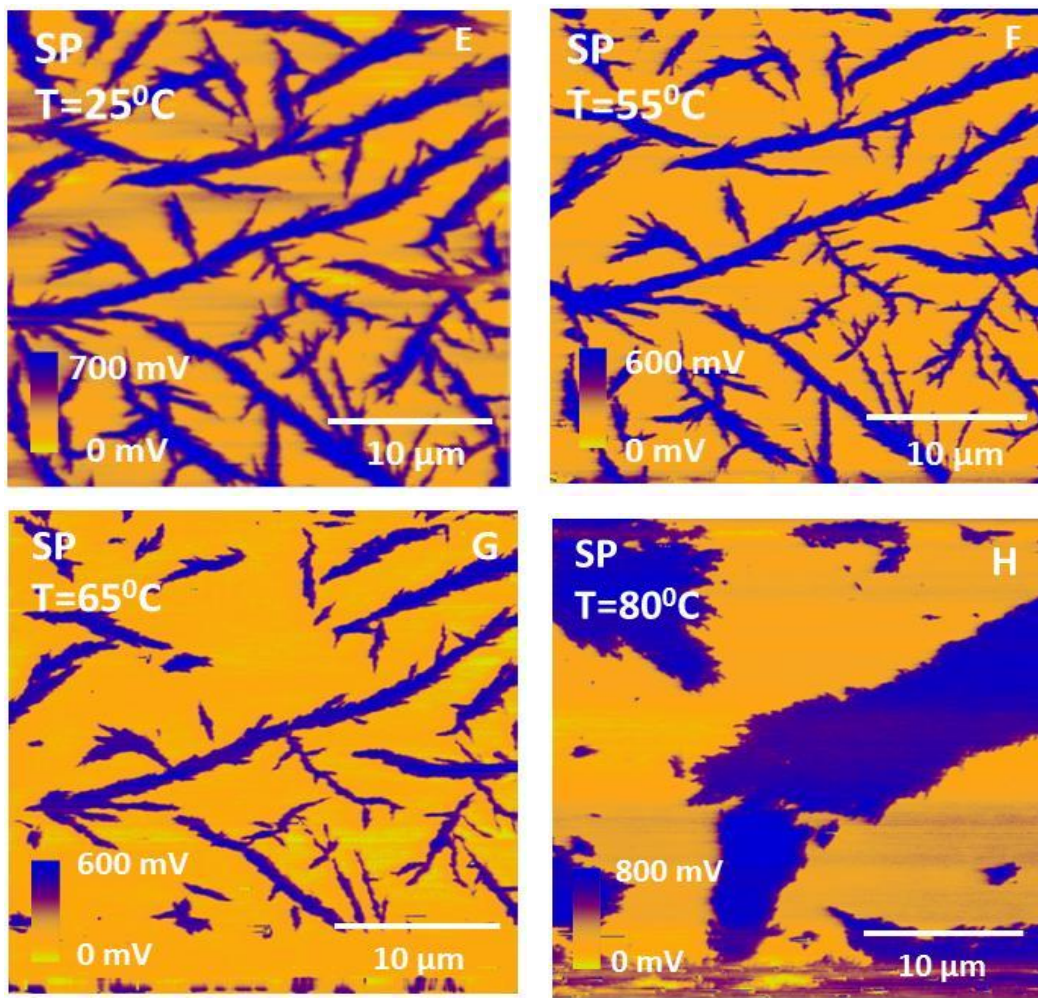


Figure 32. The contact potential differences at temperatures (A) 25<sup>0</sup>C, (B) 55<sup>0</sup>C, (C) 65<sup>0</sup>C and (D) 80<sup>0</sup>C.

Figure 31 I-L show the adhesion maps for temperature 25, 55, 65 and 80 °C, respectively. The fusing of domains at higher temperature can be explained from these adhesion maps in Figures 31I, J, K and L for temperatures 25, 55, 65 and 80 °C respectively. The graph in Figure 33 shows Adhesion as a function of temperature. A gradual increase in the adhesion of the aggregates can be observed until 55°C, however the adhesion reaches a maximum at 65°C. This indicates a change in the phase from solid or glass to liquid state. The adhesion continues to increase until the temperature of 100°C due to an increase in the viscosity of the domains. At this temperature, the domains become so mobile that imaging in the same location may not give significant information on the domains investigated at room temperature. Also, it was observed that the tip starts to get contaminated at higher temperatures due to the increased viscosity of the asphaltene aggregates.

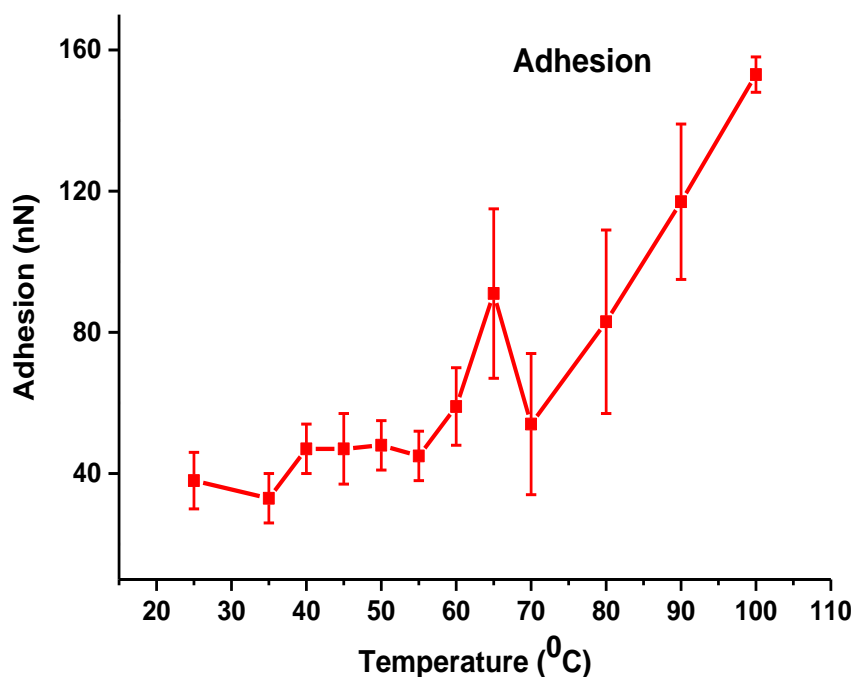
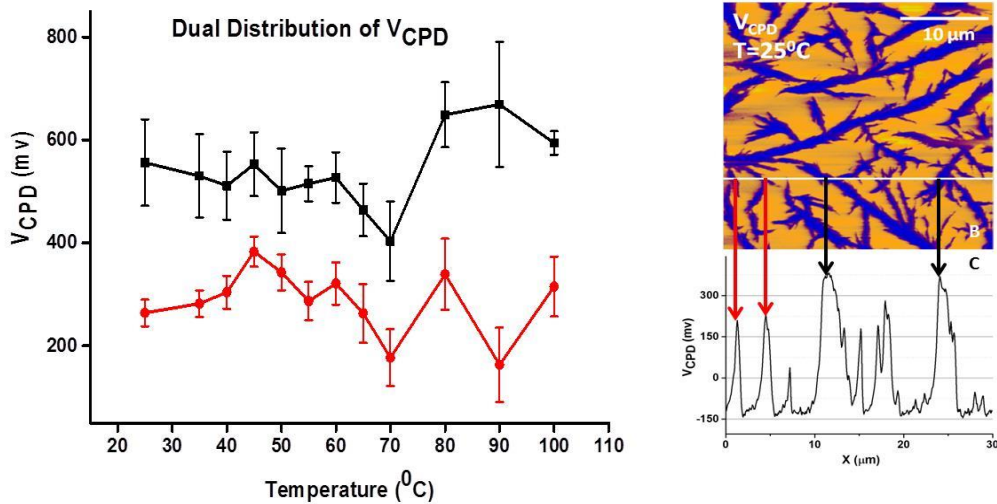


Figure 33. Asphaltenes adhesion as a function of temperature.

In order to understand whether the change in phase of asphaltene aggregates have any effect on the change in work function of the asphaltenes aggregates, a plot of contact potential difference ( $V_{CPD}$ ) between the AFM probe and asphaltene aggregates as a function of temperature is shown in Figure 34.

It is elucidating to observe a dual distribution of  $V_{CPD}$  whereby the distribution with higher values ( $\sim 500\text{mV}$ ) is for the thicker branches while the one with lower values ( $\sim 300\text{mV}$ ) is for the smaller branches. It is clearly shown in the adjacent image with its cross sectional graph aligned in proper scale just below it.



**Figure 34. Contact potential difference ( $V_{CPD}$ ) between the AFM probe and asphaltene aggregates as a function of temperature (A),  $V_{CPD}$  image of asphaltene aggregates (B) and cross section of image shown in B to identify dual distribution of  $V_{CPD}$  for hair like and broader structures. The red and black arrows indicate lower and higher  $V_{CPD}$  distribution respectively.**

One of the interesting observations in the  $V_{CPD}$  is that at  $45^{\circ}\text{C}$ , the domains tend to orient such that the  $V_{CPD}$  increases for both the distributions, however a significant decrease is seen at temperature of  $70^{\circ}\text{C}$  at which similar changes in the adhesion is observed at around  $65^{\circ}\text{C}$  as seen in Figure 33. It should be noted that the dual behavior for  $V_{CPD}$  is purely from the asphaltene aggregates having the

same height in both the large and smaller branches and has no effect due to difference in asphaltene volume.

Asphaltenes are known to be solid at room temperature, but show a transition from solid or glass state to a liquid state at higher temperatures. Depending on the nature of the asphaltene, this transition temperature can vary from several hundreds of degree Celsius<sup>90</sup> to merely few tens of degree Celsius<sup>91</sup>. In order to confirm the phase change from solid to viscous state obtained from AFM measurements, heat capacity for asphaltene was measured as part of this work. A differential scanning calorimeter TG-DSC 111 (Setaram, France) was used for heat capacity determination in the temperature range from 20 °C to 200 °C. This calorimeter is a heat flux DSC, operating on the Tian–Calvet principle and using a cylinder type measuring system comprising two cylindrical tubes set parallel and symmetrically in a heating furnace.

Temperature calibration was performed using indium, tin, lead, zinc, naphthalene and gallium. The heat capacity,  $C_p$ , calibration was performed using synthetic sapphire. The uncertainty of the  $C_p$  measurements was estimated to be less than 2% in the temperature from 20 to 200 °C. All heat capacity data were achieved using a continuous three step method (empty, reference material (sapphire) and asphaltene sample) in a measuring cell. The measuring cell was empty in the first run and filled with sapphire and the asphaltene sample in the second and third runs, respectively. The reference cell was empty during all runs. The measurements were carried out with a heating rate of 5 K.min<sup>-1</sup> followed by isothermal delays of 3600 s at the beginning and the end of each experiment. The typical mass of samples was about 50 mg (with uncertainty of 0.05 mg). The hermetically sealed stainless steel cells (the maximum pressure of 10 MPa at 573K) were utilized for all experiments. The tightness of the cells was checked before and after each trial. No mass loss of the samples was detected in any of the experiments. The collected signals from DSC includes heat capacity in J/(g.K) and temperature in °C.

The heat capacity of the asphaltene samples was calculated using the software provided for the DSC instrument. Two successive measurement runs were performed on each sample, one to obtain the initial heat capacity when asphaltene is heated. The sample is cooled back to the room temperature and again the heat capacity is measured to check the reversibility of the heat capacity values. Figure 35 shows the specific heat capacities for the first initial heating cycle 1 (red) and heating of the same sample after cooled back to room temperature cycle 2 (blue).

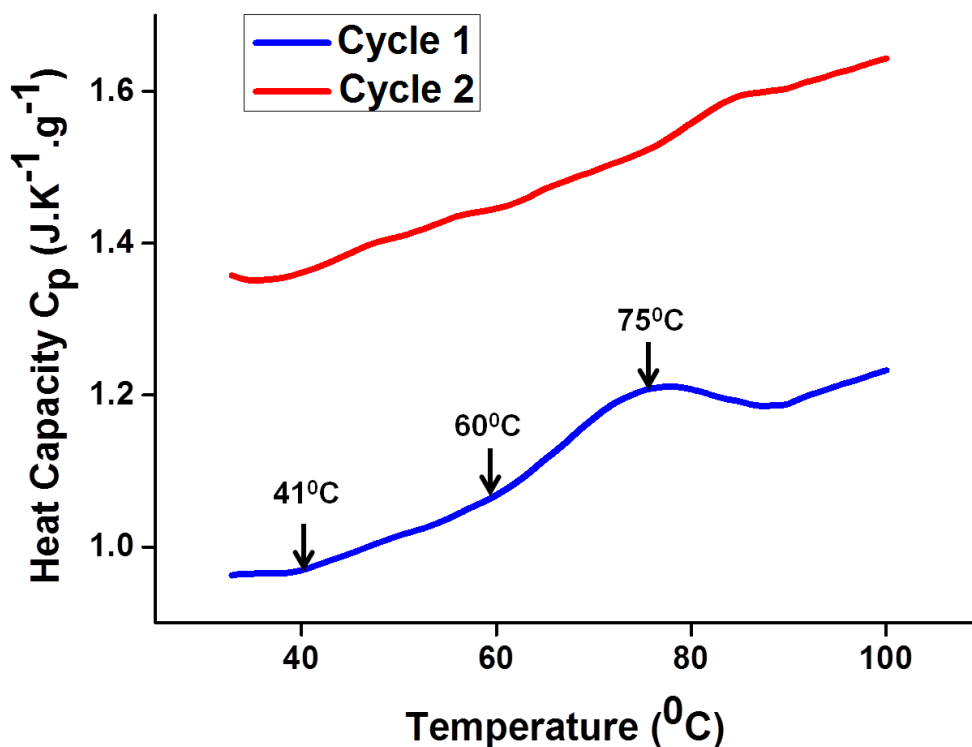


Figure 35. The specific heat capacities of asphaltene samples for the first initial heating cycle 1 (red) and heating of the same sample after cooling it down back to room temperature cycle 2 (blue). Two glass transition temperatures were identified for the first heating cycle ( $T_{G1}=41^{\circ}\text{C}$  and  $T_{G2}=60^{\circ}\text{C}$ ) and there is endothermic to exothermic phase transition at  $T=75^{\circ}\text{C}$ . For the second heating cycle there may be several glass transition temperatures, but no endothermic to exothermic phase transition temperature.

From the first heating cycle, one can clearly identify multiple glass transition temperature ( $T_G$ ). For example, for the temperature range corresponding to which the changes in asphaltene morphology was investigated, we got  $T_{G1}=41$  °C and  $T_{G2}=60$  °C. The most interesting observation of DSC thermogram is the presence of the exothermic phase transition starting at 75°C. This phase transition is the signature of the presence of a small crystalline fraction that melts in the studied temperature range and can successfully explain dynamics of asphaltene aggregates caused by their liquid-like behavior at temperatures higher than 70 °C. In order to make sure that our DSC study is representing a physically consistent picture, we performed a second heating cycle. For the second heating cycle, the apparent heat capacities are different from the first heating cycle. The specific heat capacities are consistently higher during the second heating cycle and liquid crystal domains are absent. This observation is perfectly consistent with results corresponding to second heating cycle of chemically separated asphaltenes<sup>92</sup>. The initial change in the phase transition at 60°C matches to the value at which we observe the change in the adhesion as well as the  $V_{CPD}$ . This proves that the orientation of asphaltene domains during phase transition are responsible for a change in the adhesion,  $V_{CPD}$  and hence fusing of domains at higher temperatures.

## Chapter 4

### Conclusion and Future Work

Asphaltenes are complex molecules that are loosely defined by their solubility characteristics. They are soluble in aromatic hydrocarbons such as toluene or benzene, whereas insoluble in saturated hydrocarbons such as pentane, hexane or heptane. Asphaltenes are considered the most problematic component during production and processing of heavy oils and bitumen.

Asphaltenes have very high affinity for surfaces. In this thesis we have investigated the adsorption and aggregation behaviors of asphaltenes on surfaces. Fundamental understanding the adsorption and aggregation behavior of asphaltenes are important in preventing fouling of equipment and pipelines.

In chapter 2, we have investigated the ability of the dodecanethiol SAM to prevent adsorption of asphaltenes on surfaces. Using different tethering scheme for SAM, it may be possible to coat different surfaces with SAM for preventing asphaltene adsorption. The FT-IR and ellipsometry show negligible asphaltene adsorption on the SAM coated surfaces. Findings of this research can be applied for different metals used in petroleum pipeline in order to protect them against asphaltene adsorption.

In chapter 3, a new mode Kelvin Probe Force Microscopy (KPFM), which is Peak Force-KPFM (PF-KPFM), was used to detect changes in the physical parameters of asphaltene aggregates as a function of temperature. The KPFM provides topographical images along with surface potential map with high spatial resolution and high sensitivity (potential). The morphology of asphaltene, surface potential difference and adhesion changes are investigated as a function of temperature. The height distribution of these fern-like structures changes

depending on the temperature and the effective mean height of the asphaltene domains decreases when the temperature is increased.

The adhesion reaches a maximum at 65<sup>0</sup>C. It shows that temperature increasing leads to transition from self-assembled fractal structure to larger mobile liquid-like domains. We denote such a temperature-dependent coalescence of the asphaltene aggregates as a new type of asphaltene aggregation, which occurs on account of phase transition of the existing asphaltene aggregates. Change in phase of asphaltene aggregates, also, affects the contact potential differences between tip and aggregates of asphaltene as a function of temperature. The dynamics of asphaltene aggregates at higher temperatures can be explained by transition from amorphous to liquid crystalline phase.

Future studies can be carried out to understand the dynamics of asphaltene model compounds as a function of temperature and concentration on different substrates using AFM.

The real time study of asphaltene dynamics can be studied using Fast scan mode, which has capability to record data at video rates (~100Hz). This will allow in-situ tracking of asphaltene domains as a function of temperature. This method can also be used for understanding the fusing mechanism of these domains at higher temperatures.

It may be possible to functionalize AFM tips with specific functional group to determine the local chemistry of asphaltene at nanoscale. It may also be possible to carry out the AFM investigations under solvents.

In order to sort asphaltene particles by size, dielectrophoresis cell can be used to characterize size sorted asphaltene using AFM.

## Literature Cited

- (1) Lesueur, D. *Advances in colloid and interface science* **2009**, *145*, 42–82.
- (2) Zahabi, A. Flocculation of silica particles in amodel oil solution: Effect of adsorbed asphaltene, University of Alberta, 2011.
- (3) Mullins, O. C. *SPE Journal* **2008**, 48–57.
- (4) Chang, C.; Fogler, H. S. *Langmuir* **1994**, *10*, 1749–1757.
- (5) Liao, Z.; Zhao, J.; Creux, P.; Yang, C. *Energy & Fuels* **2009**, *23*, 6272–6274.
- (6) Rahmani, N. H. G.; Dabros, T.; Masliyah, J. H. *Energy & Fuels* **2005**, *94*, 1099–1108.
- (7) Rahmani, N. H. G.; Dabros, T.; Masliyah, J. H. *Journal of colloid and interface science* **2005**, *285*, 599–608.
- (8) Rahmani, N. H. G.; Dabros, T.; Masliyah, J. H. *Industrial & Engineering Chemistry Research* **2005**, *44*, 75–84.
- (9) Gray, M. R.; Tykwinski, R. R.; Stryker, J. M.; Tan, X. *Energy & Fuels* **2011**, *25*, 3125–3134.
- (10) Karimi, A.; Qian, K.; Olmstead, W. N.; Freund, H.; Yung, C.; Gray, M. R. *Energy & Fuels* **2011**, *25*, 3581–3589.
- (11) Yen, T. F.; Chilingarian, G. V. *Asphaltenes and asphalts, 2 Developements in petroleum science, 40B*; Elsevier, 2000.
- (12) Yarranton, H. W. *Journal of Dispersion Science and Technology* **2005**, *26*, 5–8.

- (13) Yarranton, H. W.; Alboudwarej, H.; Jakher, R. *Industrial & Engineering Chemistry Research* **2000**, *39*, 2916–2924.
- (14) Souza, R. D. S.; Nicodem, D. E.; Garden, S. J.; Corrêa, R. J. *Energy & Fuels* **2010**, *24*, 1135–1138.
- (15) Gawrys, K. L.; Spiecker, P. M.; Kilpatrick, P. K. *Petroleum Science and Technology* **2003**, *21*, 461–489.
- (16) Fenistein, D.; Barre, L.; Broseta, D.; Espinat, D.; Livet, A.; Roux, J. N.; Scarsella, M. *Langmuir* **1998**, *7463*, 1013–1020.
- (17) Mostowfi, F.; Indo, K.; Mullins, O. C.; McFarlane, R. *Energy & Fuels* **2009**, *23*, 1194–1200.
- (18) Dechaine, G. P.; Gray, M. R. *Energy & Fuels* **2011**, *25*, 509–523.
- (19) Evdokimov, I. N.; Eliseev, N. Y.; Akhmetov, B. R. *Fuel* **2003**, *82*, 817–823.
- (20) Groenzin, H.; Mullins, O. C. *Energy & Fuels* **2000**, *14*, 677–684.
- (21) Sztukowski, D. M.; Jafari, M.; Alboudwarej, H.; Yarranton, H. W. *Journal of Colloid and Interface Science* **2003**, *265*, 179–186.
- (22) Espinat, D.; Fenistein, D.; Barre, L.; Frot, D.; Briolant, Y. *Energy & Fuels* **2004**, *18*, 1243–1249.
- (23) Yen, T. F.; Boucher, L. J.; Dickie, J. P.; Tynan, E. C.; Vauchan, G. B. *Journal of the Institute of Petroleum* **1969**, *55*, 87–99.
- (24) Sjoblom, J.; Aske, N.; Auflem, I. H.; Brandal, Ø.; Havre, T. E.; Saether, Ø.; Westvik, A.; Johnsen, E. E.; Kallevik, H. *Advances in Colloid and Interface Science* **2003**, *102*, 399–473.

- (25) Kilpatrick, P.; Spiecker, M. *Asphaltene emulsions. Encyclopedic handbook of emulsion technology*; CRC Press, 2001; pp. 707–730.
- (26) Mullins, O.; Sheu, E. Y. *Structures and dynamics of asphaltenes*; Springer: New York, 1998.
- (27) Wang, S. *Understanding Stability of Water-in-Diluted Bitumen Emulsions by Colloidal Force Measurement*, University of Alberta, 2011.
- (28) Rogel, E.; Leon, O.; Torres, G.; Espidel, J. *Fuel* **2000**, 79, 1389–1394.
- (29) Mohamed, R. S.; Ramos, A. C. S.; Loh, W. *Energy & Fuels* **1999**, 13, 323–327.
- (30) Andersen, S. I.; Birdi, K. S. *Journal of colloid and interface science* **1991**, 142, 497–502.
- (31) Oh, K.; Ring, T. a.; Deo, M. D. *J. Colloid Interface Sci.* **2004**, 271, 212–219.
- (32) Merino-Garcia, D.; Andersen, S. I. *Journal of Dispersion Science and Technology* **2005**, 26, 217–225.
- (33) Kuznicki, T.; Masliyah, J. H.; Bhattacharjee, S. *Energy & Fuels* **2008**, 22, 2379–2389.
- (34) Aray, Y.; Hernández-Bravo, R.; Parra, J. G.; Rodríguez, J.; Coll, D. S. *The journal of physical chemistry. A* **2011**, 115, 11495–507.
- (35) Boduszynski, M. M. *In chemistry of asphaltenes*; American Chemical Society: Washington, D.C., 1981; p. Chapter 7.
- (36) Andersen, S. I. *Fuel Science and Technology Int'l.* **1994**, 12, 51–74.
- (37) Mullins, O. C. *Energy & Fuels* **2009**, 23, 2845–2854.

- (38) Schneider, M. H.; Andrews, A. B.; Mitra-Kirtley, S.; Mullins, O. C. *Energy & Fuels* **2007**, *21*, 2875–2882.
- (39) Nordgård, E. L.; Sjöblom, J. J. *Dispersion Sci. Technol.* **2008**, *29*, 1114–1122.
- (40) Jaffe, S. B.; Freund, H.; Olmstead, W. N. *Ind. Eng. Chem. Res.* **2005**, *44*, 9840–9852.
- (41) Kawanaka, S.; Leontaritis, K. J.; Park, S. J.; Mansoori, G. A. In *ACS symposium series*; Washington, DC, 1989; pp. 443–458.
- (42) Agrawala, M.; Yarranton, H. W. *Ind. Eng. Chem. Res.* **2001**, *40*, 4664–4672.
- (43) Ancheyta, J.; Betancourt, G.; Centeno, G.; Marroqui, G.; Alonso, F.; Garciafiguroa, E. *Energy & Fuels* **2002**, *16*, 1438–1443.
- (44) Katz, D. L.; Beu, K. E. *Industrial & Engineering Chemistry* **1945**, *37*, 195–200.
- (45) Preckshot, G. W.; DeLisle, N. G.; Cottrell, C. E.; Katz, D. L. *Trans. AIME* **1943**, *151*, 188.
- (46) Lichaa, P. M.; Herrera, L. In *SPE Oilfield Chemistry Symposium*; Society of Petroleum Engineers: Dallas, Texas, 1975.
- (47) Fotland, P.; Anfindsen, H.; Fadnes, F. H. *Fluid Phase Equilibria* **1993**, *82*, 157–164.
- (48) Parra-Barraza, H.; Hernández-Montiel, D.; Lizardi, J.; Hernández, J.; Urbina, R. H.; Valdez, M. A. *Fuel* **2003**, *82*, 869–874.
- (49) Kokal, S.; Tang, T.; Schramm, L.; Sayegh, S. *Colloids and Surfaces A: Physicochemical and Engineering Aspects* **1995**, *94*, 253–265.

- (50) Vega, S. S.; Urbina, R. H.; Covarrubias, M. V.; Galeana, C. L. *Journal of Petroleum Science and Engineering* **2009**, *69*, 174–180.
- (51) Das, S.; Thundat, T.; Mitra, S. K. *Fuel* **2013**, *108*, 543–549.
- (52) Gonzalez, G.; Neves, G. B. M.; Saraiva, S. M.; Lucas, E. F.; De Sousa, M. dos A. *Energy & Fuels* **2003**, *17*, 879–886.
- (53) Alboudwarej, H.; Pole, D.; Svrcek, W. Y.; Yarranton, H. W. *Industrial & Engineering Chemistry Research* **2005**, *44*, 5585–5592.
- (54) Rahmani, N. H. G.; Dabros, T.; Masliyah, J. H. *Chemical Engineering Science* **2004**, *59*, 685–697.
- (55) Dudášová, D.; Simon, S.; Hemmingsen, P. V.; Sjöblom, J. *Colloids and Surfaces A: Physicochemical and Engineering Aspects* **2008**, *317*, 1–9.
- (56) Trejo, F.; Centeno, G.; Ancheyta, J. *Fuel* **2004**, *83*, 2169–2175.
- (57) Ancheyta, J.; Betancourt, G.; Marroqu, G.; Centeno, G.; Castañeda, L. C.; Alonso, F.; Muñoz, J. A.; Gómez, M. T.; Rayo, P. *Applied Catalysis A: General* **2002**, *233*, 159–170.
- (58) Leontaritis, K. J.; Kawanaka, S.; Mansoori, G. A. In *ACS Symposium on Advances in Oil Field Chemistry*; 1988; pp. 196–204.
- (59) Dickakian, G.; Seay, S. *Oil and Gas Journal* **1988**, *86*, 47–50.
- (60) Toulhoat, H.; Prayer, C.; Rouquet, G. *Colloids and Surfaces A: Physicochemical and Engineering Aspects* **1994**, *91*, 267–283.
- (61) Drummond, C.; Israelachvili, J. *Journal of Petroleum Science and Engineering* **2004**, *45*, 61–81.

- (62) Akhlaq, M. S.; Gtze, P.; Kessel, D.; Dornow, W. *Colloids and Surfaces A: Physicochemical and Engineering Aspects* **1997**, *126*, 25–32.
- (63) Labrador, H.; Fernandez, Y.; Tovar, J.; Munoz, R.; Pereira, J. C. *Energy & Fuels* **2007**, 1226–1230.
- (64) Batina, N.; Reyna-Cordova, A.; Trinidad-Reyes, Y.; Quintana-Garcia, M.; Buenrostro-Gonzalez, E.; Lira-Galeana, C.; Andersen, S. I. *Energy & Fuels* **2005**, *19*, 2001–2005.
- (65) Ekholm, P.; Blomberg, E.; Claesson, P.; Auflem, I. H.; Sjöblom, J.; Kornfeldt, A. *Journal of colloid and interface science* **2002**, *247*, 342–50.
- (66) Turgman-Cohen, S.; Fischer, D. a; Kilpatrick, P. K.; Genzer, J. *ACS applied materials & interfaces* **2009**, *1*, 1347–57.
- (67) Hannisdal, A.; Ese, M.-H.; Hemmingsen, P. V.; Sjöblom, J. *Colloids and Surfaces A: Physicochemical and Engineering Aspects* **2006**, *276*, 45–58.
- (68) Turgman-Cohen, S.; Smith, M. B.; Fischer, D. a; Kilpatrick, P. K.; Genzer, J. *Langmuir : the ACS journal of surfaces and colloids* **2009**, *25*, 6260–9.
- (69) Ulman, A. *Chemical reviews* **1996**, *96*, 1533–1554.
- (70) Park, J.-S.; Vo, A. N.; Barriet, D.; Shon, Y.-S.; Lee, T. R. *Langmuir : the ACS journal of surfaces and colloids* **2005**, *21*, 2902–11.
- (71) Love, J. C.; Estroff, L. a; Kriebel, J. K.; Nuzzo, R. G.; Whitesides, G. M. *Self-assembled monolayers of thiolates on metals as a form of nanotechnology.*; 2005; Vol. 105, pp. 1103–69.
- (72) Porter, M. D.; Bright, T. B.; Allara, D. L.; Chidsey, C. E. D. *American Chemical Society* **1987**, 3559–3568.

- (73) Peng, M. Thermal cracking of asphaltene by adding of hydrogen donor solvent, University of Alberta, 2010.
- (74) Godin, M.; Williams, P. J.; Tabard-Cossa, V.; Laroche, O.; Beaulieu, L. Y.; Lennox, R. B.; Grütter, P. *Langmuir* **2004**, *20*, 7090–6.
- (75) Vericat, C.; Vela, M. E.; Benitez, G.; Carro, P.; Salvarezza, R. C. *chemical Society Reviews* **2010**, 1805–1834.
- (76) Coates, J. *Interpretation of infrared spectra, a practical approach*; 2000; pp. 10815–10837.
- (77) Bertilsson, L.; Liedberg, B. *Langmuir* **1993**, 141–149.
- (78) Coelho, R. R.; Hovell, I.; Monte, M. B. D. M.; Middea, A.; Souza, A. L. *De Fuel Processing Technology* **2006**, *87*, 325–333.
- (79) Calemma, V.; Iwanski, P.; Nali, M.; Scotti, R.; Montanari, L. *Energy & Fuels* **1995**, 225–230.
- (80) Wilt, B. K.; Welch, W. T.; Rankin, J. G. *Energy & Fuels* **1998**, *0624*, 1008–1012.
- (81) Michels, R.; Langlois, E.; Ruau, O.; Mansuy, L.; Elie, M.; Landais, P. *Energy & Fuels* **1996**, 477–486.
- (82) Fujiwara, H. *spectroscopic ellipsometry: principles and applications*; Wiley, 2007.
- (83) Butt, H.-J.; Cappella, B.; Kappl, M. *Surface Science Reports* **2005**, *59*, 1–152.
- (84) Binnig, G.; Quate, C. F. *Physical Review Letters* **1986**, *56*, 930–934.

- (85) Sourty, E. D.; Tamminga, A. Y.; Michels, M. A. J.; Vellinga, W.-P.; Meijer, H. E. H. *Journal of microscopy* **2011**, *241*, 132–46.
- (86) Melitz, W.; Shen, J.; Kummel, A. C.; Lee, S. *Surface Science Reports* **2011**, *66*, 1–27.
- (87) Domanski, A. L.; Sengupta, E.; Bley, K.; Untch, M. B.; Weber, S. a L.; Landfester, K.; Weiss, C. K.; Butt, H.-J.; Berger, R. *Langmuir* **2012**, *28*, 13892–13899.
- (88) Yasutake, M.; Aoki, D.; Fujihira, M. *Thin Solid Films* **1996**, *273*, 279–283.
- (89) Zerweck, U.; Loppacher, C.; Otto, T.; Grafström, S.; Eng, L. *Physical Review B* **2005**, *71*, 125424.
- (90) Yasar, M.; Akmaz, S.; Ali Gurkaynak, M. *Fuel* **2007**, *86*, 1737–1748.
- (91) Tran, K. Q. Reversing and non-reversing phase transitions in athabasca bitumen asphaltenes, University of Alberta, 2009.
- (92) Bazyleva, A.; Fulem, M.; Becerra, M.; Zhao, B.; Shaw, J. M. *J. Chem. Eng. Data* **2011**, *56*, 3242–3253.